1980

ADVANCED GAS TURBINE (AGT) POWERTRAIN SYSTEM DEVELOPMENT PROGRAM

CONTRACT NUMBER DEN3-167

2-24-81
3-27-81
8/27/82

ELEVENTH MONTHLY
TECHNICAL PROGRESS REPORT
FOR THE PERIOD
AUGUST 1, 1980 THROUGH AUGUST 31, 1980

AIRESEARCH MANUFACTURING COMPANY OF ARIZONA
A DIVISION OF THE GARRETT CORPORATION
111 SO. 34TH STREET, PHOENIX, ARIZONA

AUTHOR: R.A. RACKLEY

REPORT NO. 31-3480(11)
SEPTEMBER 26, 1980

PREPARED FOR
NASA/LEWIS RESEARCH CENTER
CLEVELAND, OHIO 44135

ADVANCED GAS TURBINE
(AGT)
POWERTRAIN SYSTEM DEVELOPMENT
CONTRACT NO. DEN3-167
ELEVENTH MONTHLY TECHNICAL
PROGRESS REPORT
AUGUST 1, 1980 THROUGH AUGUST 31, 1980

31-3480(11) September 26, 1980

Prepared by J. E. Galligan, J. P. Brosman

Initial Issue
Approved by R. A. Rackley
R. A. Rackley
AGT Project Manager

E. E. Strain
E. E. Strain,
AGT Program Manager

AIRESEARCH MANUFACTURING COMPANY OF ARIZONA
A DIVISION OF THE GARRETT CORPORATION
PHOENIX, ARIZONA

REPORT NO. 31-3480 (11)

TOTAL PAGES 54

ATTACHMENTS: Appendix I
Appendix II
Appendix III
Appendix IV

REV	BY	APPROVED	DATE	PAGES AND/OR PARAGRAPHS AFFECTED
N/C	JEG	See Title Page	9-26-80	Eleventh Monthly Progress Report

TABLE OF CONTENTS

TABLE OF CONTENTS (Contd)

AIRESEARCH MANUFACTURING COMPANY OF ARIZONA
A DIVISION OF THE GARRETT CORPORATION
PHOENIX, ARIZONA

ELEVENTH MONTHLY TECHNICAL PROGRESS REPORT FOR THE AIRESEARCH ADVANCED GAS TURBINE (AGT) POWERTRAIN SYSTEM DEVELOPMENT PROGRAM

1.0 INTRODUCTION

This report, submitted by AiResearch Manufacturing Company of Arizona, a Division of The Garrett Corporation, presents the Eleventh Monthly Technical Progress Report for the Advanced Gas Turbine (AGT) Powertrain System Development Program, authorized under NASA Contract DEN3-167 sponsored by the Department of Energy (DOE). The program is administered by Mr. Roger Palmer, Project Manager NASA Lewis Research Center, Cleveland, Ohio, Telephone (216) 433-4000. Work reported herein covers the reporting period of August 1, 1980 through August 31, 1980.

Effort conducted under this contract is part of the DOE Gas Turbine Highway Vehicle Systems Program, which is aimed at providing the United States automotive industry the technology base necessary to produce gas turbine powertrains for automobiles having reduced fuel consumption and reduced environmental impact. It is intended that technology resulting from this program be capable of reaching the marketplace by the early 1990's.

This specific contract effort is directed toward the principal DOE program objective, which is to develop an experimental AGT powertrain system by 1985 that has a metro/highway fuel economy of 41 mpg on diesel fuel, the same driveability as a conventionally powered vehicle, emission levels meeting Federal standards, and multi-fuel capability.

The AGT Program Schedule and AGT Program Major Milestones are shown in Figure 1-1 and 1-2, respectively.

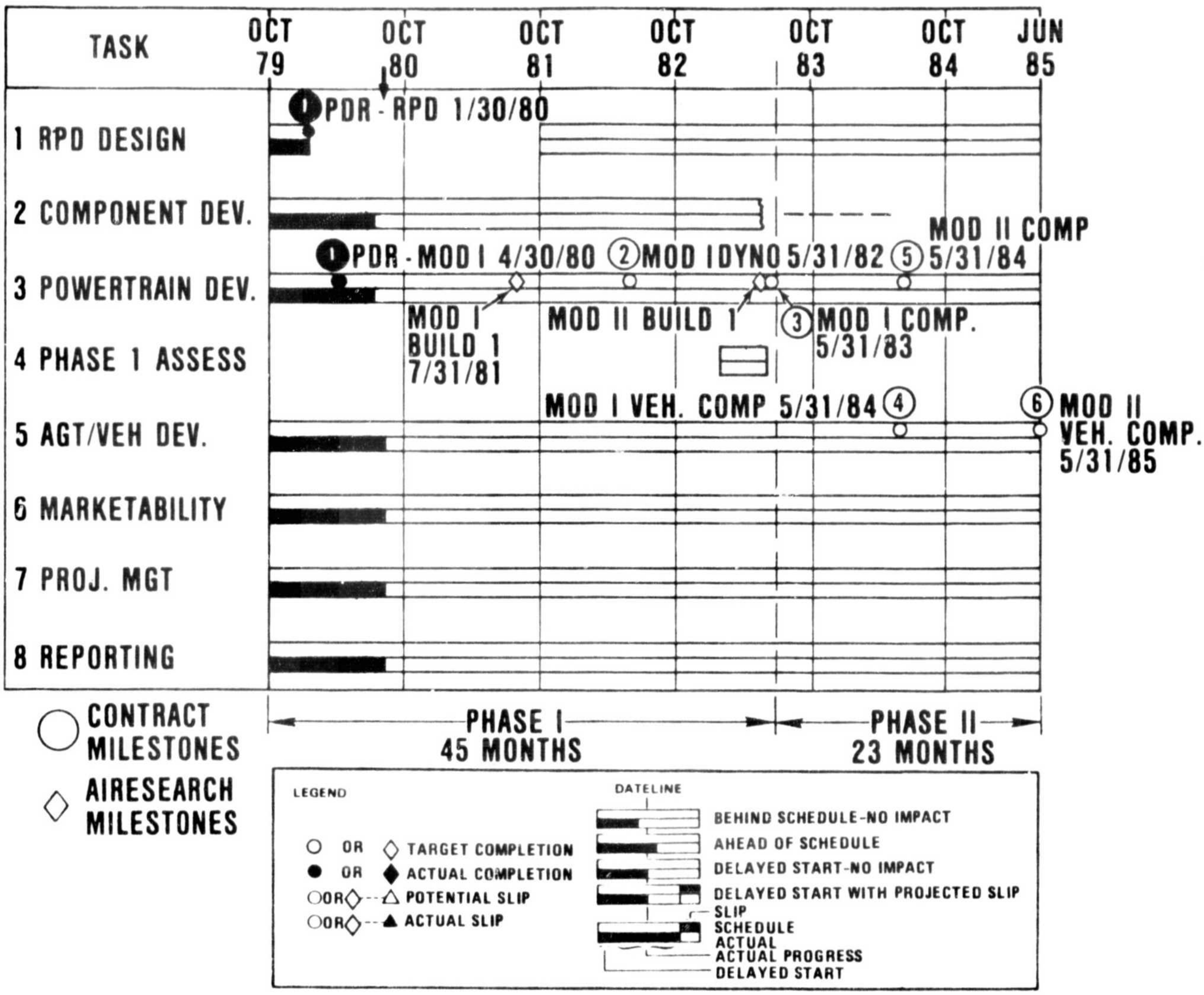

Figure 1-1. AGT101 Project Schedule.

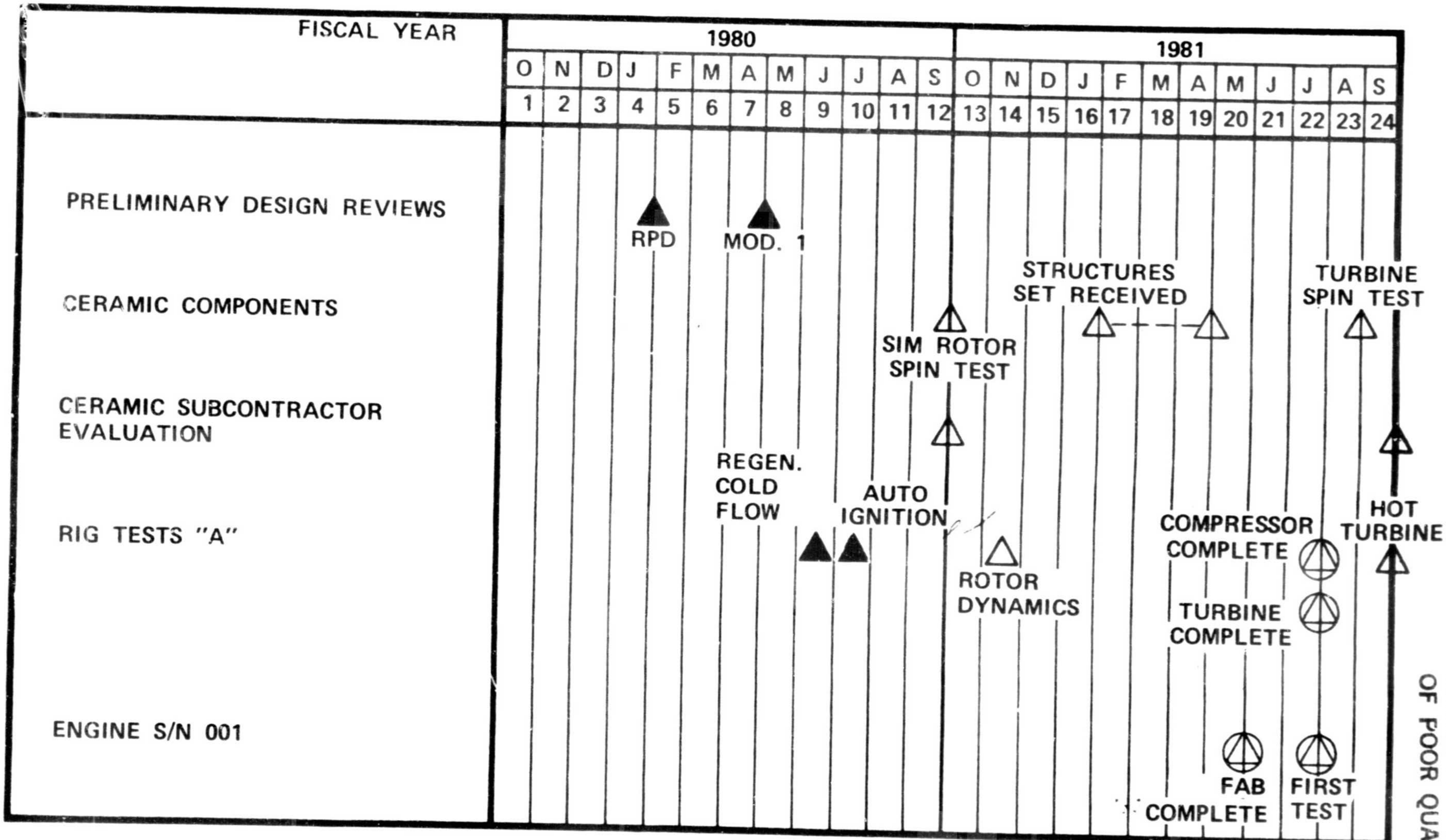

Figure 1-2. AGT101 Major Milestones.

2.0 TECHNICAL PROGRESS SUMMARY

The following paragraphs describe the monthly activities for AGT program tasks with discussion provided for each component/subsystem, as applicable.

2.1 Task 1.0 - AGT101 Reference Powertrain Design (RPD)

The AGT101 RPD was completed on January 30, 1980. No additonal Task 1.0 activity is expected until 1982.

2.2 Task 2.0 - Component/Subsystem Development

Discussions concerning the compressor, turbine, combustor, regenerator, gearbox, ceramic components/subsystems, bearings, and controls are presented in the following paragraphs.

2.2.1 Compressor

2.2.1.1 Aerodynamics

No activity in August.

2.2.1.2 Materials

2.2.1.2.1 Powder Metal

Novamet IN-9081 alloy forging iterations showed no improvement in properties compared with previous results. The alloy did not respond to variations in forging parameters, temperatures and reduction ratios. Results did not provide an incentive to pursue this alloy further.

ALCOA Al-Fe-Ce alloy development has progressed very well. Mechanical properties to date meet or exceed AGT101 goals. Therefore, the program has been revised to replace Novamet IN-9081 with the ALCOA Al-Fe-Ce alloy.

All forgings will be ordered the week of September 1, 1980 for delivery in early December and will be sized for AGT101 impeller requirements.

The test program has been defined for tensile, HCF, LCF and stress rupture property testing. Spin testing will follow.

2.2.1.2.2 Abradable Coating

Test rig modifications have been completed to simulate AGT101 conditions. Flame-spray coating evaluation will proceed in September 1980 with first-phase completion by October 31, 1980. Spray coating will be applied to the test rig and first engine parts.

2.2.1.3 Compressor Test Rig

Hardware fabrication continues for both the dynamic and IGV rigs. IGV rig assembly is scheduled for late September 1980 with testing in October 1980. Compressor rig assembly and integrity testing is scheduled for completion in December 1980, with mapping tests to follow in early January 1981.

2.2.2 Turbine

2.2.2.1 Turbine Rotor

The sintered αSiC rotor detail drawing was completed by the end of August 1980. Signoff and release will be completed in early September 1980.

2.2.2.2 Test Rigs

Cold turbine design was essentially completed in August 1980. Detail release and part changes common to the stator flow rig will be completed in September 1980.

Stator flow rig detail design was initiated in August 1980. This rig will feature a high degree of commonality with the dynamic rig. A dummy turbine shell, with installed stator survey pressure probes, will be remotely controlled at the test panel. The motorized drive for compressor impeller clearance control has been adapted to provide this feature.

All rig design activity is scheduled for completion by September 30, 1980.

2.2.2.3 Dual Alloy Turbine Rotor

Two rotors were poured during August 1980 in the initial DS blade MAR-M-247 evaluation.

A photograph of rotor No. 2 displaying the grain of the DS blades is shown in Figure 2-1.

2.2.3 Combustion System

2.2.3.1 Autoignition Test Rig

A major portion of the work associated with the autoignition test rig concerned reworking the venturi fuel injector to obtain a reasonable fuel distribution from venturi-to-venturi. The initial design used 0.010 inch inner diameter fuel tubes which were flow sensitive to bends in the tube. To alleviate the problem, the 0.010 inch tubes were replaced with tubes of 0.038 inch inner diameter with welded and

ORIGINAL PAGE
BLACK AND WHITE PHOTOGRAPH

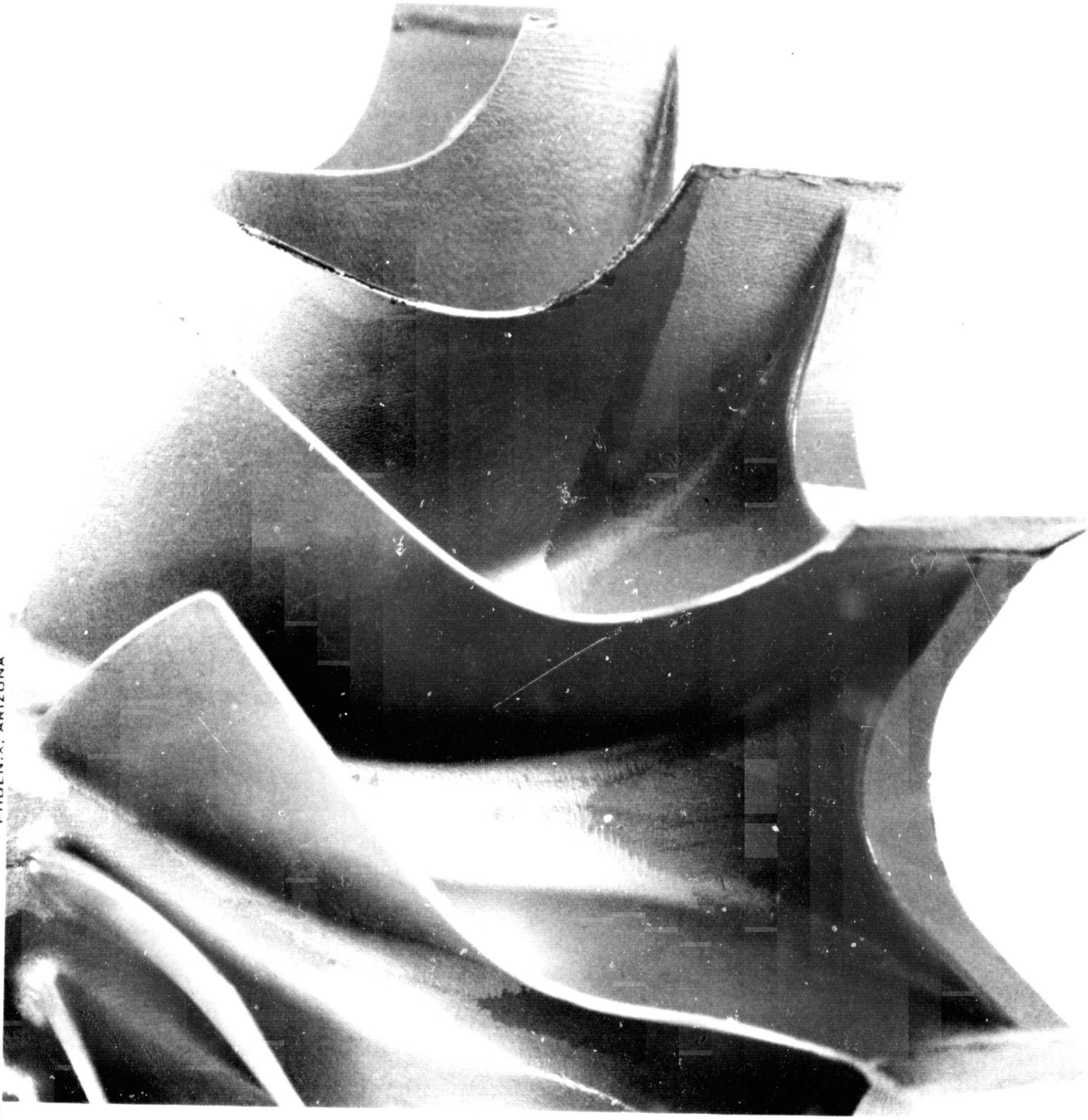

Figure 2-1. Rotor No. 2 Initial DS Blade MAR-M-247 Evaluation.

drilled ends with a 0.014 inch hole. Twenty-two tubes were individually flowed over the range of fuel flow anticipated for the autoignition testing and the thirteen best tubes were selected. These tubes were assembled in the venturi nozzle and each tube was flowed individually. After replacing one leaking tube, an average flow number of 1.51 was achieved with a +6 percent and -7.9 percent variation.

The nozzle was installed in the autoignition rig, and the rig was cold flow tested. The rig operated properly, including all of the air cooling and water cooling circuits.

Following the cold flow test, the rig was inspected and instrumentation changed in preparation for hot testing. Visual inspection of the area where the venturi nozzle discharged into the test section revealed possible recirculating areas off the nozzle exit which could affect autoignition data. To ensure that flow disturbances off the venturi would be minimal, a three inch outer diameter by two inch inner diameter alumina insulating sleeve was slipped into the test section. The sleeve blocked off the six outer venturies and minimized step changes transitioning from the venturi nozzle to the test section. Air flow to the six out venturi passages were closed by tack welding shim stock over the inlets and capping the appropriate fuel tubes.

Test points for the autoignition rig were calculated based upon data presented at the "Premixed Prevaporized Combustor Technology Forum" at NASA Lewis on January 9-10, 1979. (See Figure 2-2). A set of test points is shown in Table 2-1 where the calculated autoignition was based on Figure 2-2 data and test autoignition time is based on the inlet conditions to the test section, a 5.08 cm diameter test section, and a 30.48 cm long test section.

ORIGINAL PAGE IS
OF POOR QUALITY

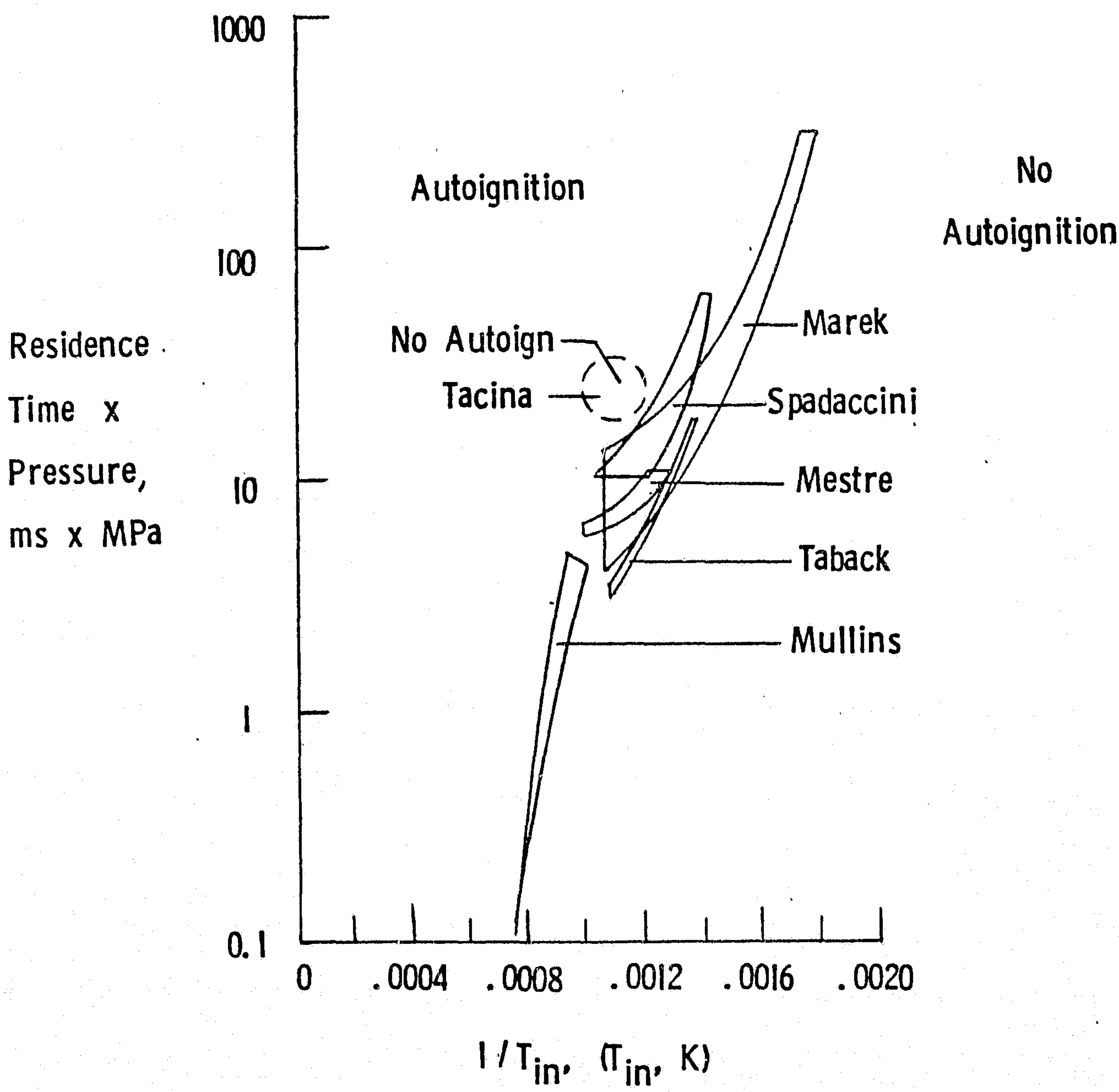

Figure 2-2. NASA Lewis Presented Autoignition Data.

TABLE 2-1. AUTOIGNITION TEST CONDITIONS

Test Point	Air Flow (lbm/sec)	Inlet Pres. (psia)	Inlet Temp (°F)	Calc. Auto Ignition Time (Millisec)	Test Auto Ignition Time (Millisec)
1	0.250	70	1100	20.0	11.0
2	0.251	70	1200	15.7	10.0
3	0.259	70	1300	10.5	9.1
4	0.561	70	1400	4.7	4.0
5	0.375	70	1400	4.7	6.0
6	0.281	70	1400	4.7	8.0
7	0.505	50	1500	3.4	3.0
8	0.304	50	1500	3.4	5.0
9	0.260	60	1500	3.4	7.0
10	0.286	30	1600	3.3	3.0
11	0.259	45	1600	3.3	5.0
12	0.268	65	1600	3.3	7.0
13	0.271	30	1700	2.0	3.0
14	0.275	50	1700	2.0	5.0
15	0.256	65	1700	2.0	7.0
16	0.264	30	1800	1.4	3.0
17	0.263	50	1800	1.4	5.0
18	0.271	32	1900	0.94	3.0
19	-.251	50	1900	0.94	5.0
20	0.256	32	2000	0.69	3.0
21	0.266	55	2000	0.69	5.0

2.2.3.2 Fuel Nozzles

Hardware to replace the venturi nozzle with the Delavan fuel nozzle design in the autoignition rig is presently being fabricated. Delavan nozzles will be tested following venturi nozzle testing.

2.2.3.3 Main Combustor Test Rig

The full scale combustor rig is presently being designed. The rig will accommodate both metal and ceramic combustors. Rig instrumentation locations have been deferred. Discharge instrumentation consists of total pressure, emissions, and temperature radial rakes. Radial rakes are mounted on a shaft that will transverse axially as well as rotate in the circumferential direction. Total pressure radial ports are manifolded, whereas the temperature and emission probes consist of five discrete ports on each rake. The emission probe head is water cooled for structural integrity and to rapidly reduce sample temperature to freeze the gas composition. The major portion of the remaining probe is fabricated of platinum to withstand high temperatures.

Static pressure tape and thermocouples will be placed in the flow annulus around the combustor to determine the uniformity of the flow passing from the 130 degree regenerator discharge to the 360 degree combustor inlet.

Both the diffusion flame combustor and the diffusion flame pilot combustor are completing detailed design. The only questionable area is the combustor-transition duct seal, which is presently being redesigned.

2.2.3.4 AGT MOD I Diffusion Flame Combustor

Efforts this month have been directed towards a modification of the Mod I Build 1 diffusion flame combustor design in order that it may be used as a backup Mod I combustor. Current activity includes analysis of this combustor using Mod I conditions and the 3-D mathematical model.

A preliminary analysis indicates that the current Mod I Build 1 design needs to have the physical open area increased from 4.0 square inches to 4.4 square inches. This increased open area is included in the four cooling bands. This will result in combustor pressure drop values of approximately 3.0 percent at cruise and 1.8 and 3.2 percent at idle and maximum power, respectively.

2.2.4 Regenerator

2.2.4.1 Regenerator LP Cold Rig

Phase I testing of the LP rig is complete. Table 2-2 provides a summary of the tests performed and includes such parameters as:

- o Diffuser Inlet Swirl
- o Corrected Flow
- o Radial and Circumferential Distortion Indices
- o Radial and Circumferential Maximum Distortion Locations

Additionally, a hole metal plate (~16 percent open area) was calibrated and installed flush against the upstream side of the core for $\Delta P/P$ simulation of the hot core.

Preliminary conclusions:

TABLE 2-2. VELOCITY DISTORTION INDICES

TEST	DESCRIPTION	SWIRL	$W\sqrt{\theta}/\delta$	RDI_{MAX}	θ	CDI_{MAX}	RADIUS
2	Baseline	-27°	1.468	1.017	160°	0.541	7.09
5	"	$+55^{\circ}$	0.33	0.487	50°	0.398	7.09
7	"	0°	0.60	0.633	50°	0.319	6.69
9	"	0°	0.33	0.556	50°	0.262	7.09
10	"	0°	1.468	0.880	50°	0.789	8.00
11	Downstream Baffle -1	0°	"	0.607	50°	0.583	7.82
12	" -2	0°	"	0.478	50°	0.621	7.82
13	" -3	0°	"	0.483	50°	0.724	7.82
14	" -4	0°	"	0.493	50°	0.710	7.82
15	Baseline w/Exhaust cover	0°	"	0.823	50°	0.452	7.82
16	Upstream Flow diverter	0°	"	0.696	50°	0.532	4.77

- Figures 2-3 and 2-4 show the influence of diffuser exit swirl on regenerator flow profiles (cold configuration). The swirl creates a minor circumferential variation in the flow patterns (i.e., slightly higher flows at both ends) that will be attenuated by core rotational effects and redistributed due to thermal effects. In any case, analysis indicates the loss in effectiveness from circumferential distortion is negligible.

- Figures 2-5 through 2-7 show the effect of variation in corrected mass flow rate on regenerator flow patterns. It can be seen in these figures that the radial velocity gradient becomes more severe as the flowrate increases (i.e., ~14 percent from idle to maximum power corrected flow). The decision was made to concentrate on the cruise corrected flow profiles based on these variations, thereby optimizing for CFDC cruise weighting.

- Figures 2-8 through 2-11 show the effect of downstream baffles as defined in Test III of Document 31-3597. The -2 configuration indicates the best compromise between flow redistribution and $\Delta P/P$. However, this data is again for the cold flow patterns and does not account for the thermally induced flow redistribution which will lower the effect of the downstream baffles. Further tests on the downstream baffle configurations are not anticipated at this time.

- Figure 2-12 shows the effect on circumferential flow profiles resulting from the installation of the exhaust manifold. Again the loss in effectiveness due to this circumferential variation in flow is negligible. No changes in the exhaust manifold configuration are currently planned.

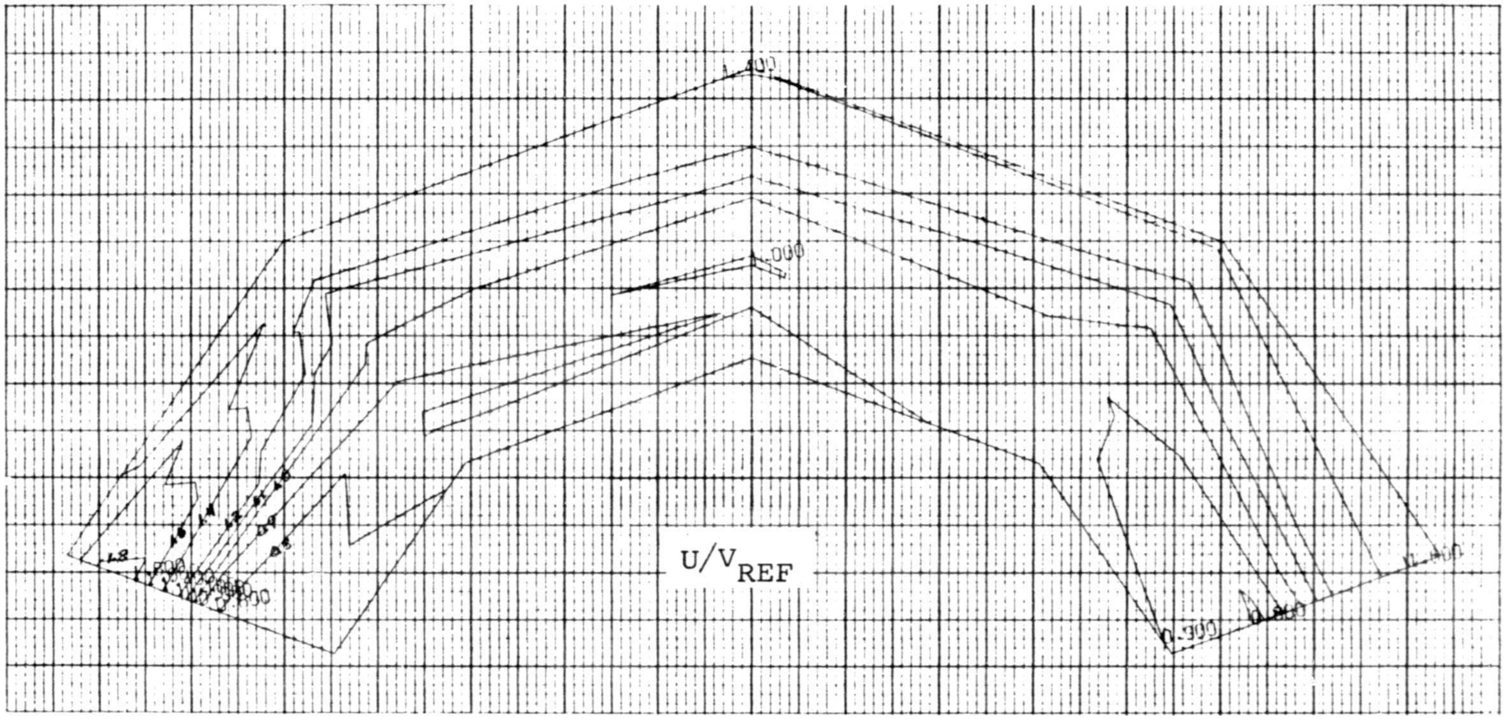

Figure 2-3. TEST NO. II-2
CONFIGURATION - BASELINE
PRESWIRL = -27°
$W\sqrt{\theta}/\delta$ = 1.468 lbm/s

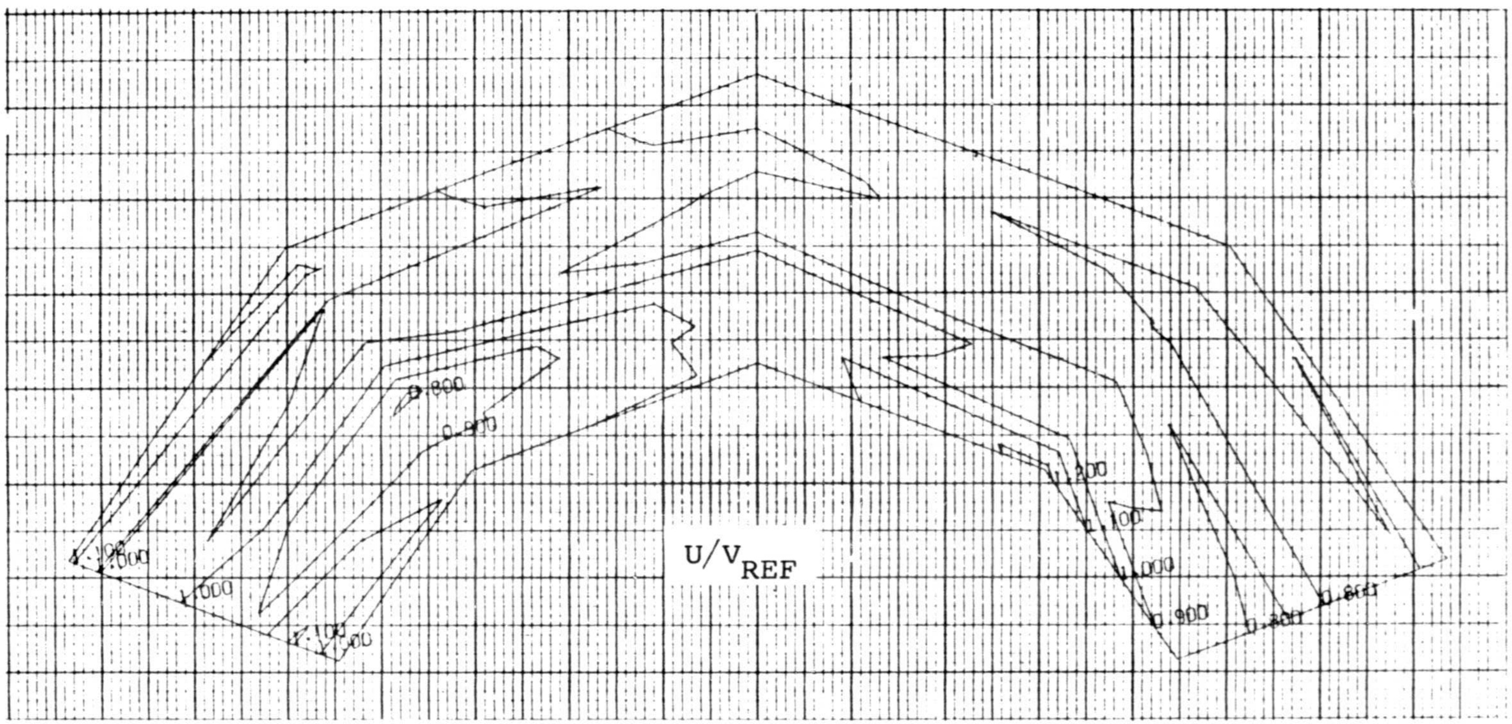

Figure 2-4. TEST NO. II-5
CONFIGURATION - BASELINE
PRESWIRL = +55°
$W\sqrt{\theta}/\delta$ = 0.33 lbm/s

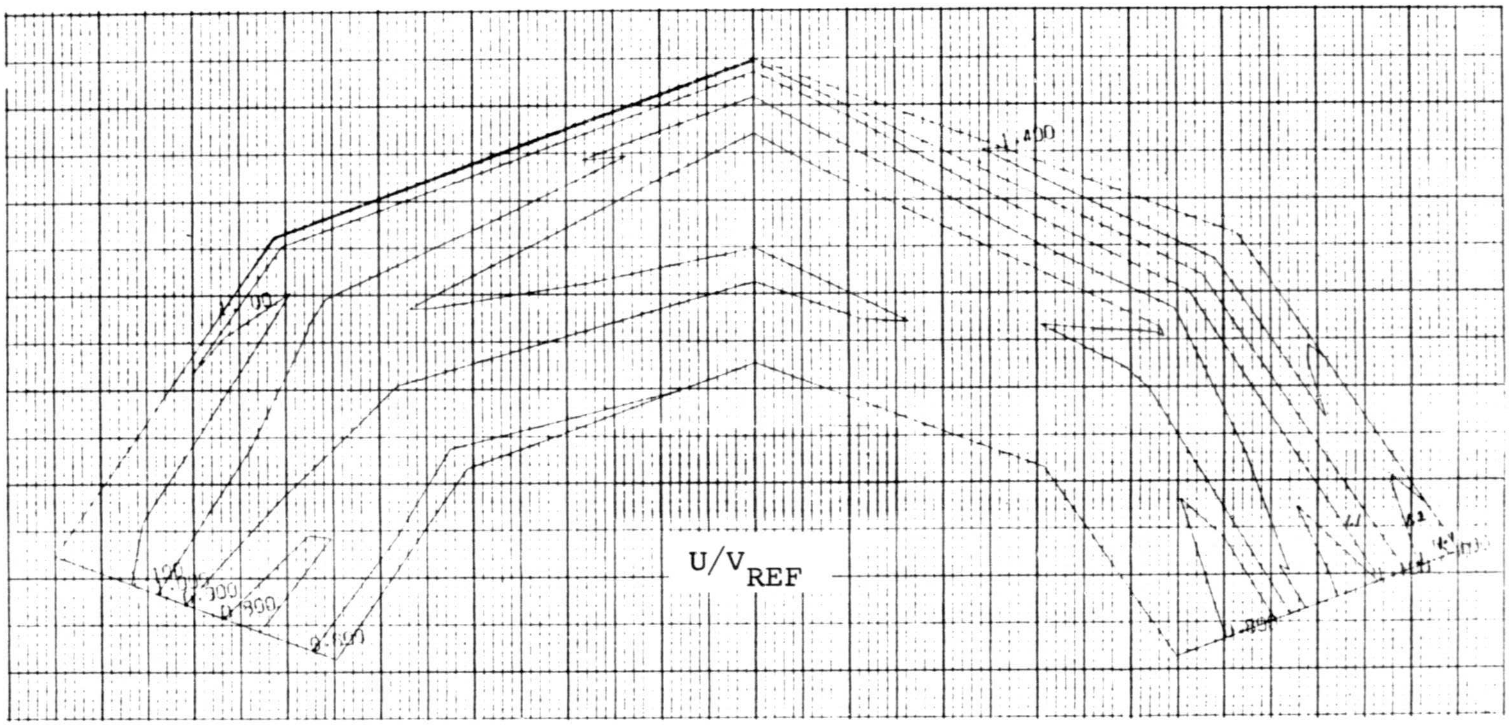

Figure 2-5. TEST NO. II-7
CONFIGURATION - BASELINE
PRESWIRL = 0°
$W\sqrt{\theta}/\delta$ = 0.6 lbm/s

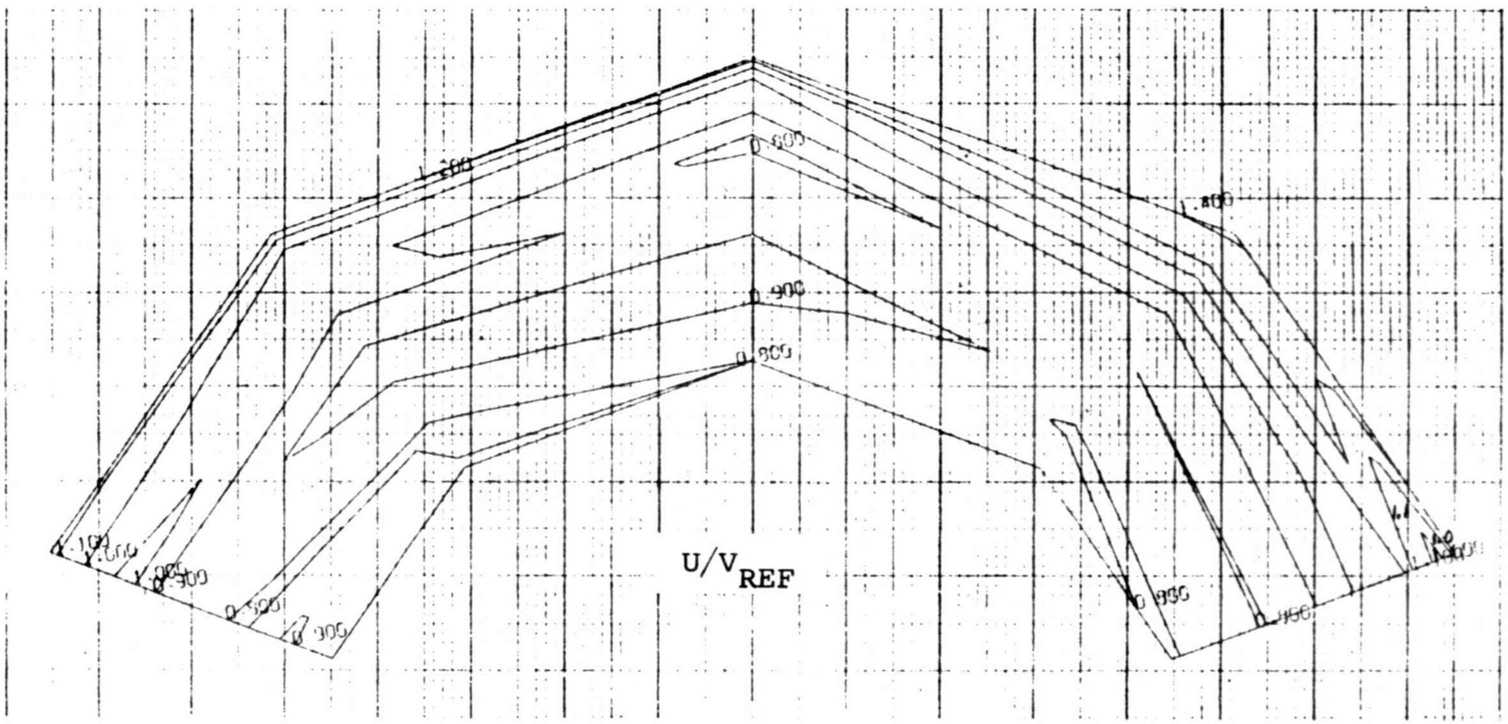

Figure 2-6. TEST NO. II-9
CONFIGURATION - BASELINE
PRESWIRL = 0°
$W\sqrt{\theta}/\delta$ = 0.33 lbm/s

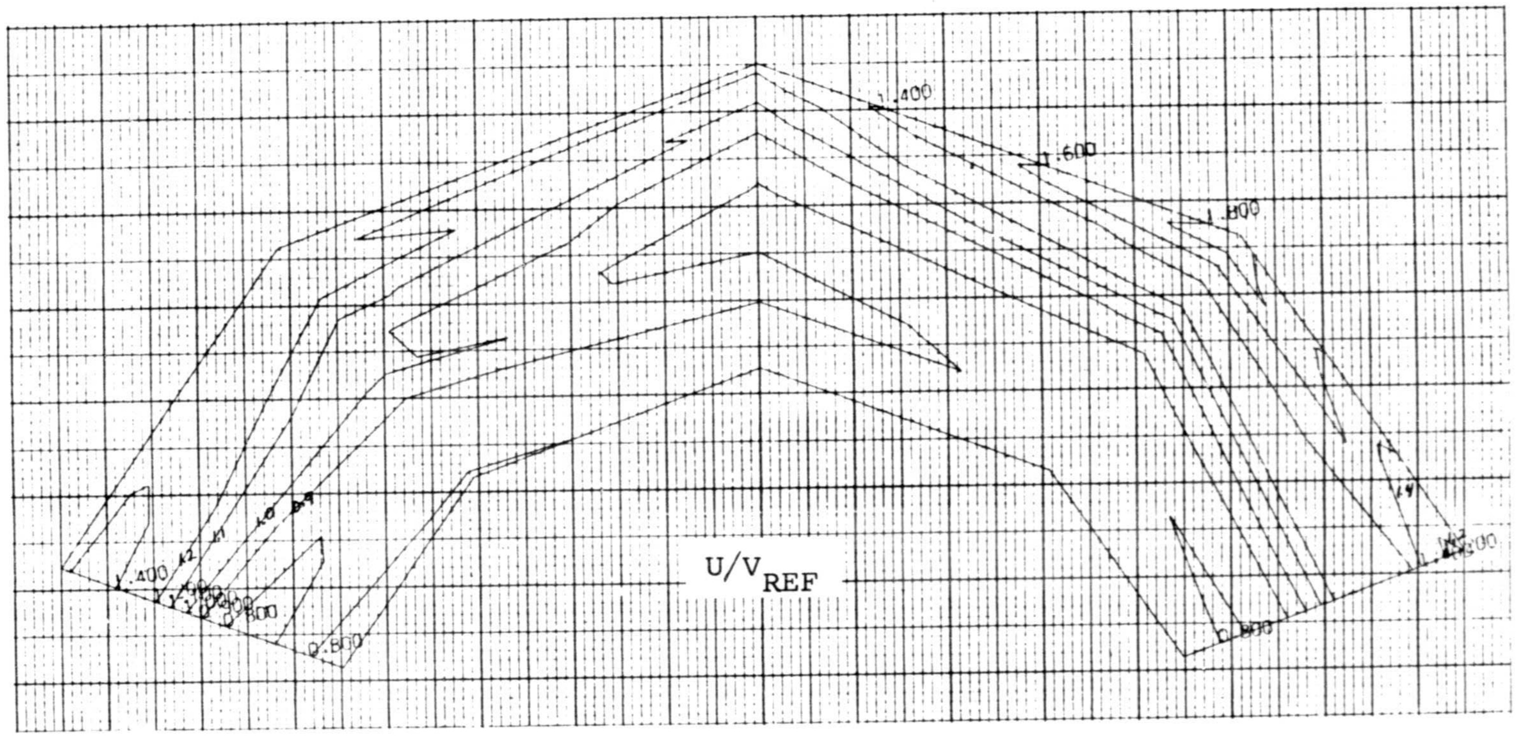

Figure 2-7. TEST NO. II-10
CONFIGURATION - BASELINE
PRESWIRL = 0°
$W\sqrt{\theta}/\delta$ = 1.468 lbm/s

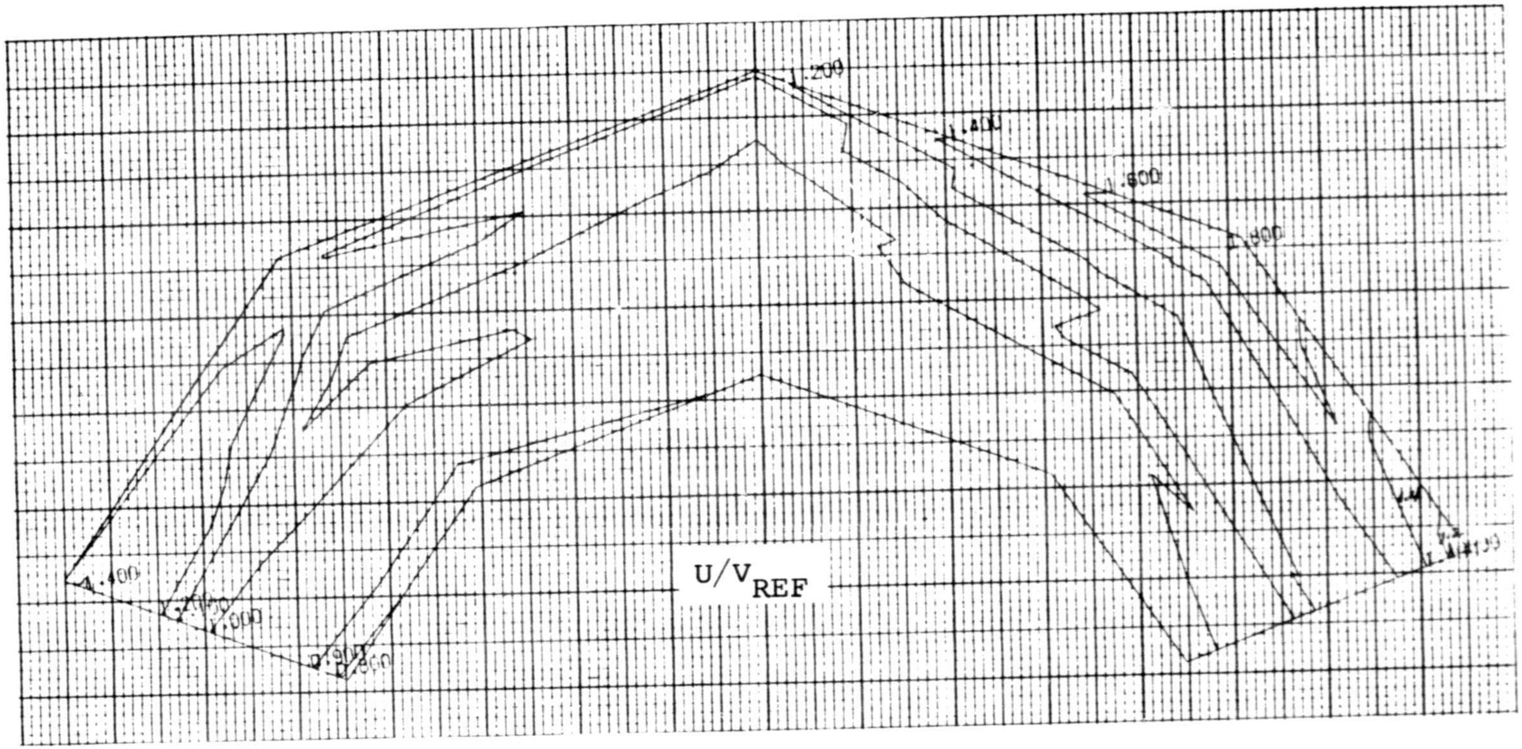

Figure 2-8. TEST NO. II-11
CONFIGURATION - DOWNSTREAM BAFFLE-1

PRESWIRL = 0°
$W\sqrt{\theta}/\delta$ = 1.468 lbm/s

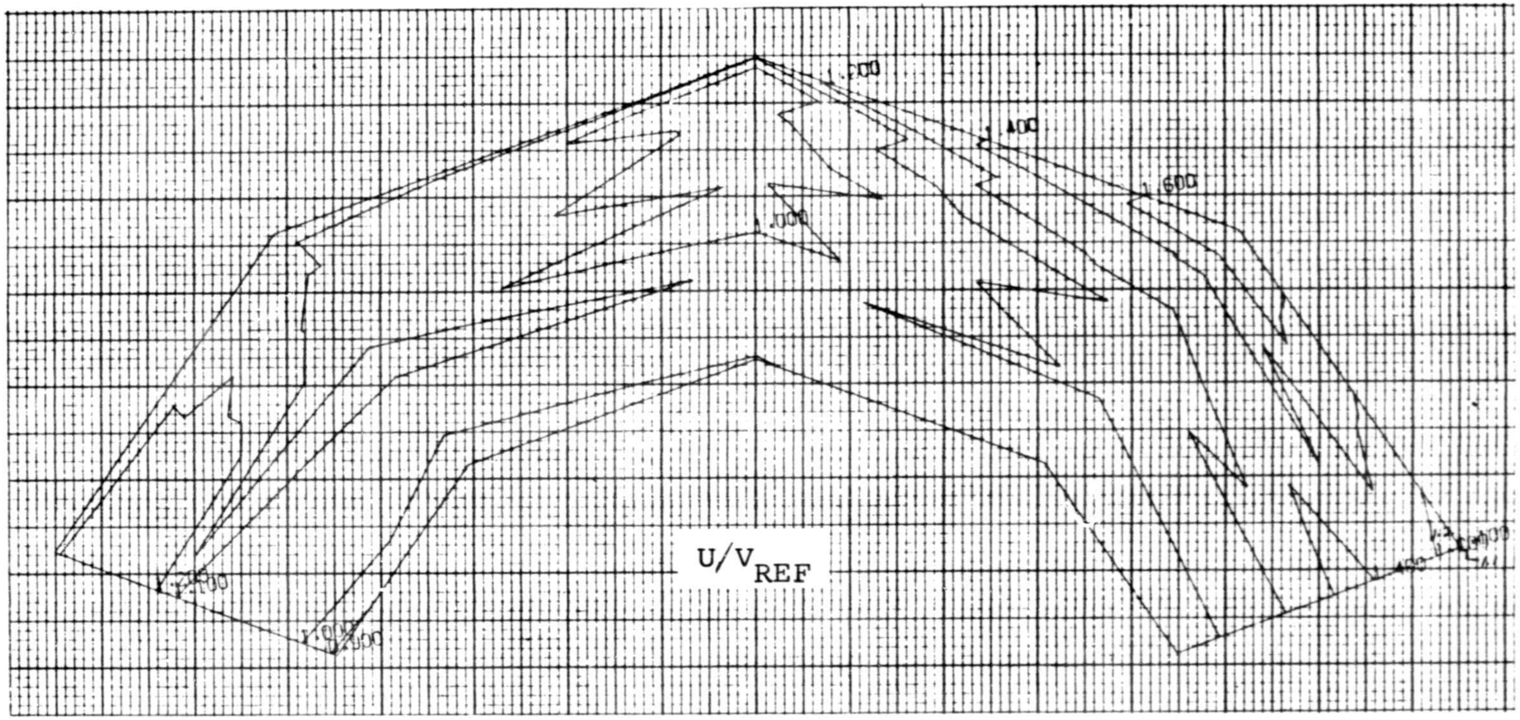

Figure 2-9. TEST NO. II-12
CONFIGURATION - DOWNSTREAM BAFFLE-2
PRESWIRL = 0°
$W\sqrt{\theta}/\delta$ = 1.468 lbm/s

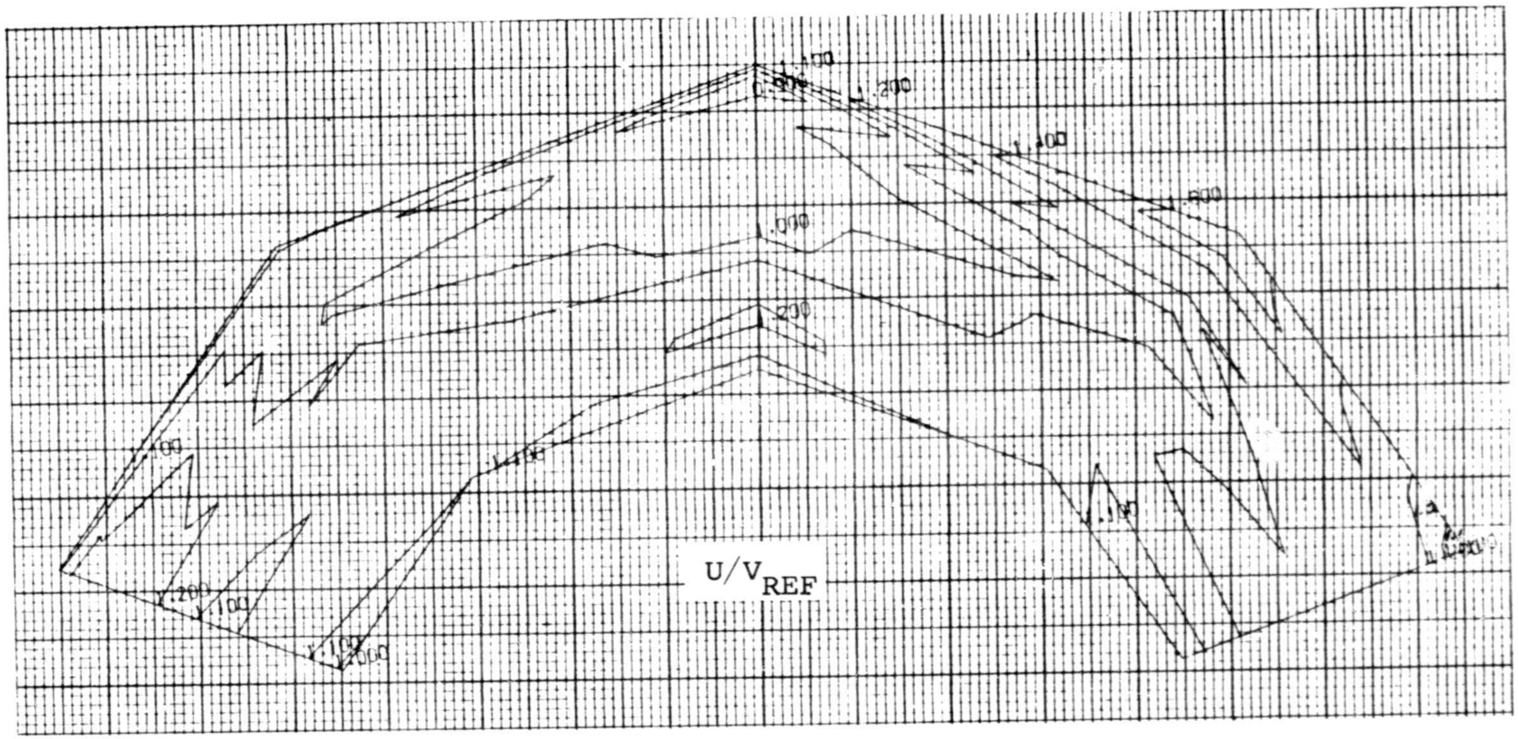

Figure 2-10. TEST NO. II-13
CONFIGURATION - DOWNSTREAM BAFFLE-3
PRESWIRL = 0°
$W\sqrt{\theta}/\delta$ = 1.468 lbm/s

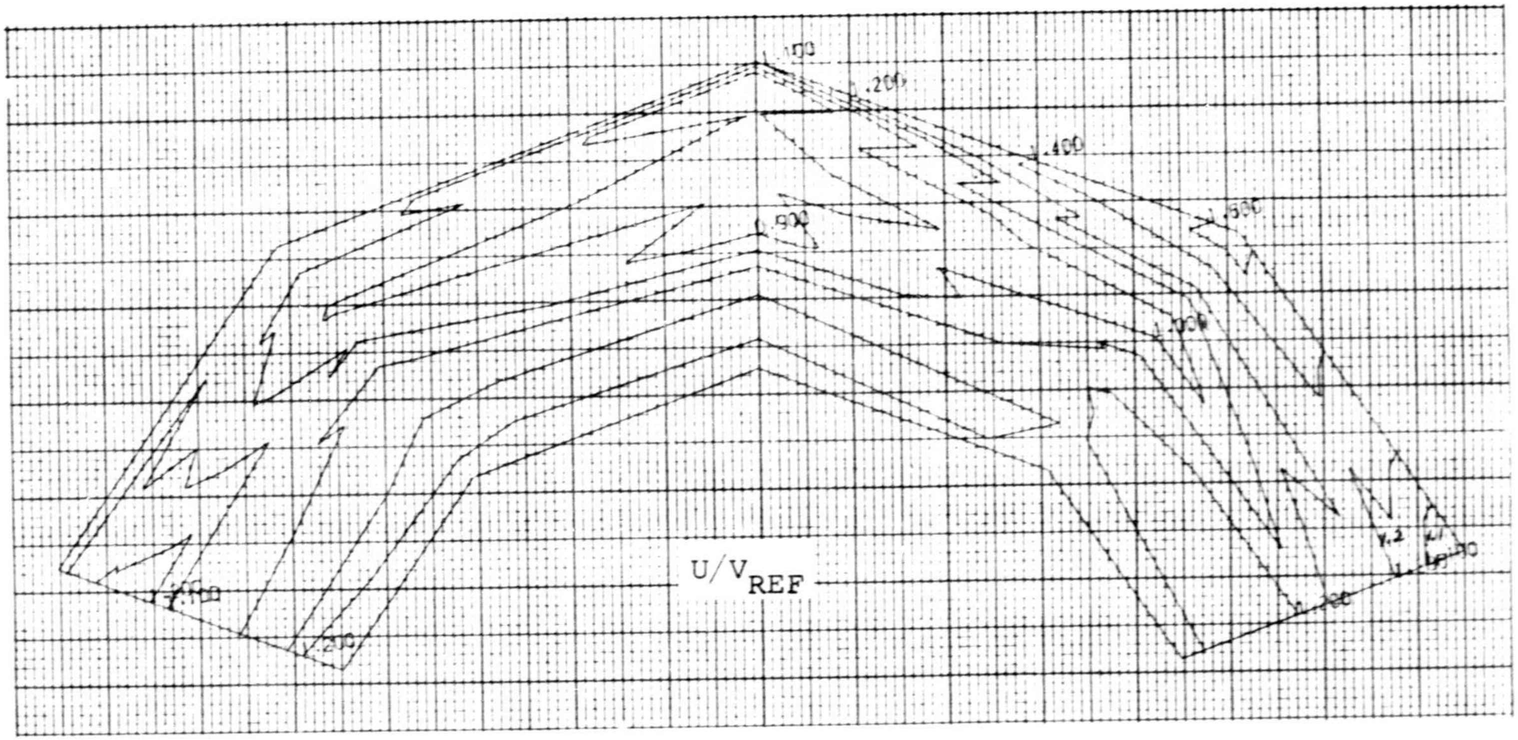

Figure 2-11. TEST NO. II-14
CONFIGURATION - DOWNSTREAM BAFFLE-4
PRESWIRL = 0°
$W\sqrt{\theta}/\delta$ = 1.468 lbm/s

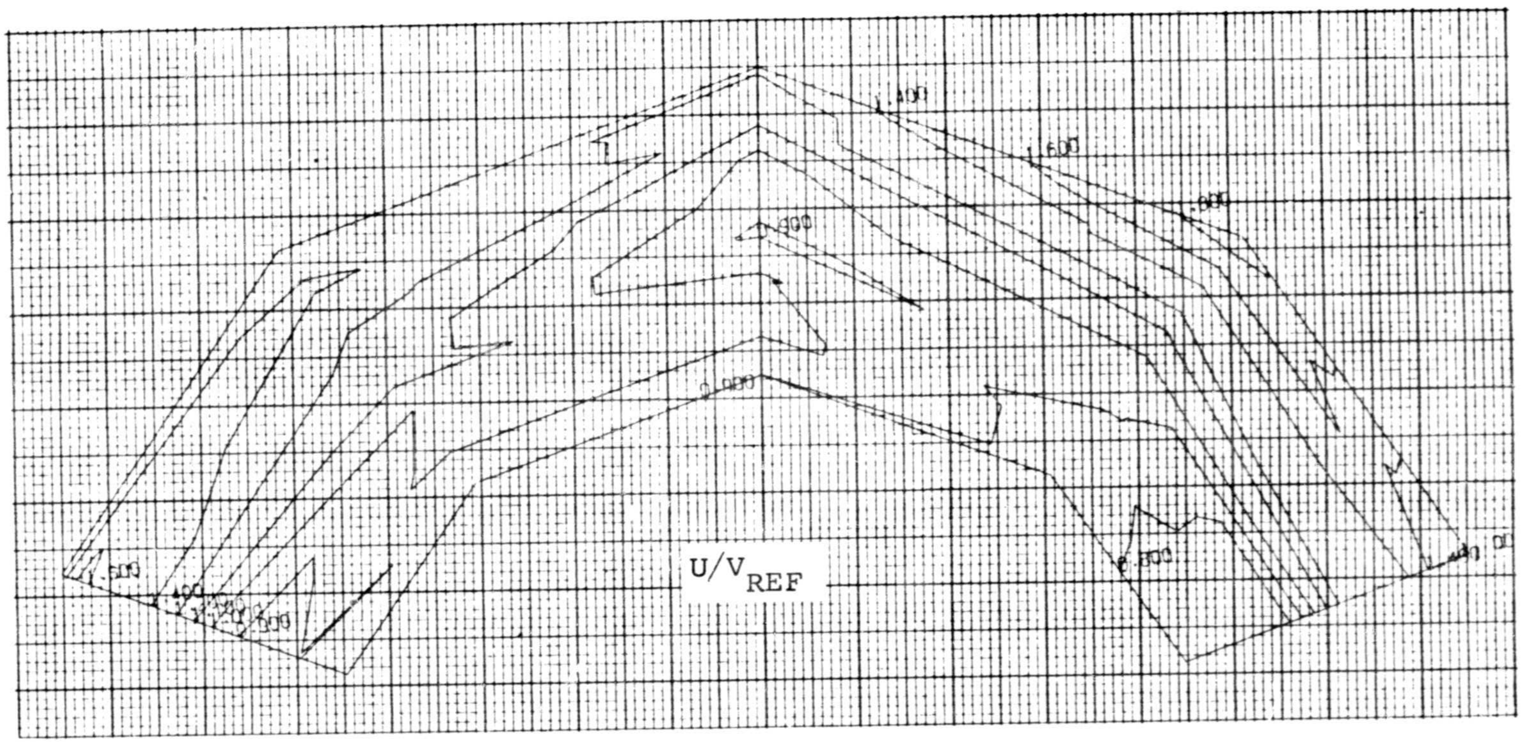

Figure 2-12. TEST NO. II-15
CONFIGURATION - BASELINE
N/EXHAUST COVER
PRESWIRL = 0°
$W\sqrt{\theta}/\delta$ = 1.468 lbm/s

- Figure 2-13 shows the effect of an upstream diverter (Figure 2-14) on the radial flow profiles. This method of redirecting the streamlines was most effective and will be pursued in Phase II testing. The exact diverter axial position and chord length is pending investigation. Phase II tests will follow HP rig tests and will focus on optimizing baffles configurations to achieve a minimum upstream radial pressure gradient.

- A stagnation pressure survey of the LP rig was conducted at cruise corrected flow by stagnating a small area of the core by applying a probe to the core discharge (Figure 2-15).

  Data from this test agrees well with the theoretical relationship between $U/V_{ref.}$ and ΔP for a uniform core matrix geometry in the cold flow rig (Figure 2-16). This method of determining flow distribution in the core appears promising for future testing where core matrix uniformity has been verified by separate test.

- Simulation of the Newton number relationship for the gas side was accomplished by the addition of a ~16 percent open area hole metal plate (Figure 2-17) to the upstream face of the core. Figure 2-18 shows how the flow was redistributed as a function of core ΔP. Stagnation pressures (inches H_2O) were again utilized as it provides the least amount of scatter in the data.

  Although a redistribution of flow is evident as a function of core ΔP the redistribution due to time dependent thermally induced ΔP is yet to be substantiated. No further cold rig testing is planned in this regard.

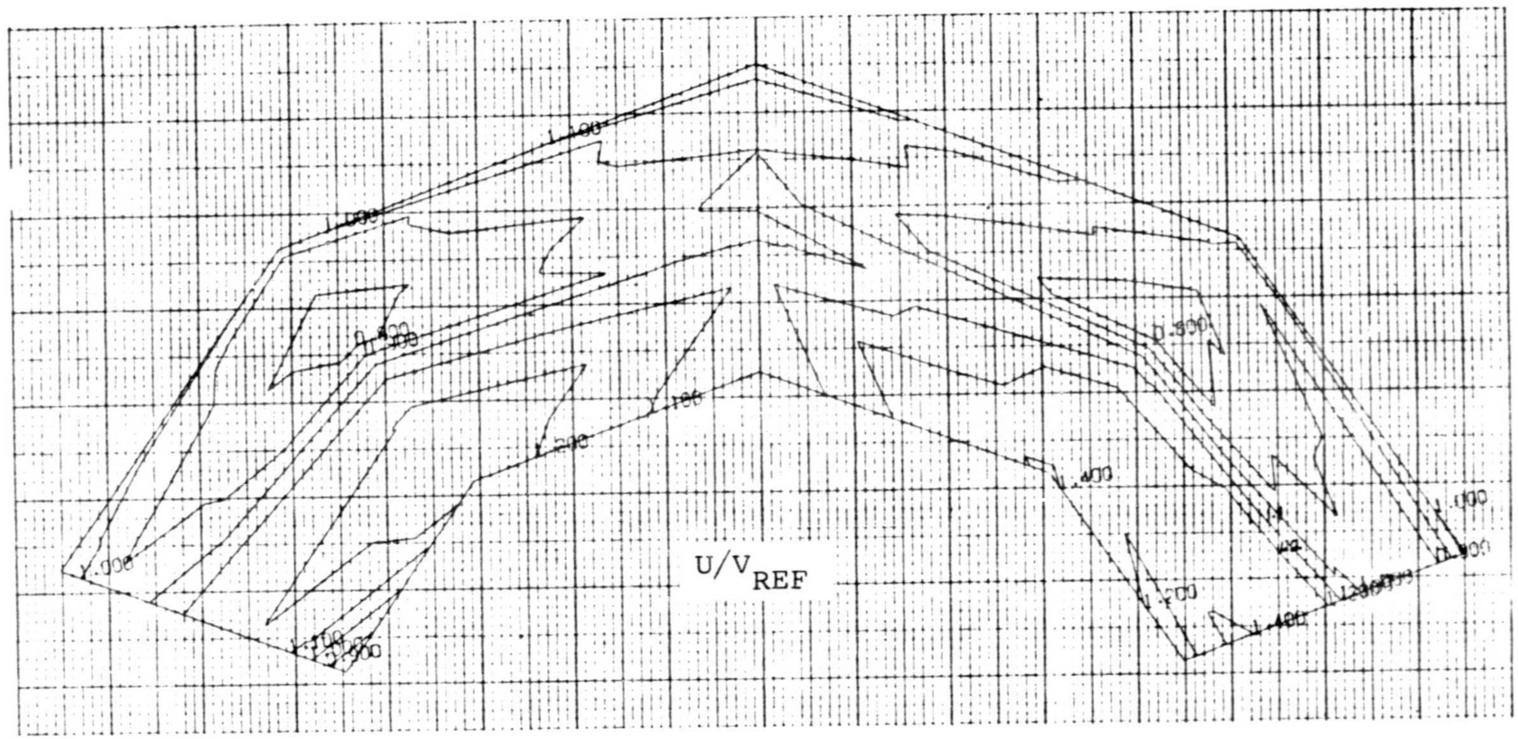

Figure 2-13. TEST NO. II-16
CONFIGURATION - UPSTREAM DIVERTER-1
PRESWIRL = 0°
$W\sqrt{\theta}/\delta$ = 1.468 lbm/s

BASELINE
CONFIGURATION
NO PLATE

TEST II
DATE 8-18-80
PRESWIRL = 0°
$W\sqrt{\theta}/\delta$ = 0.6
V_{REF} = 15 FT/SEC

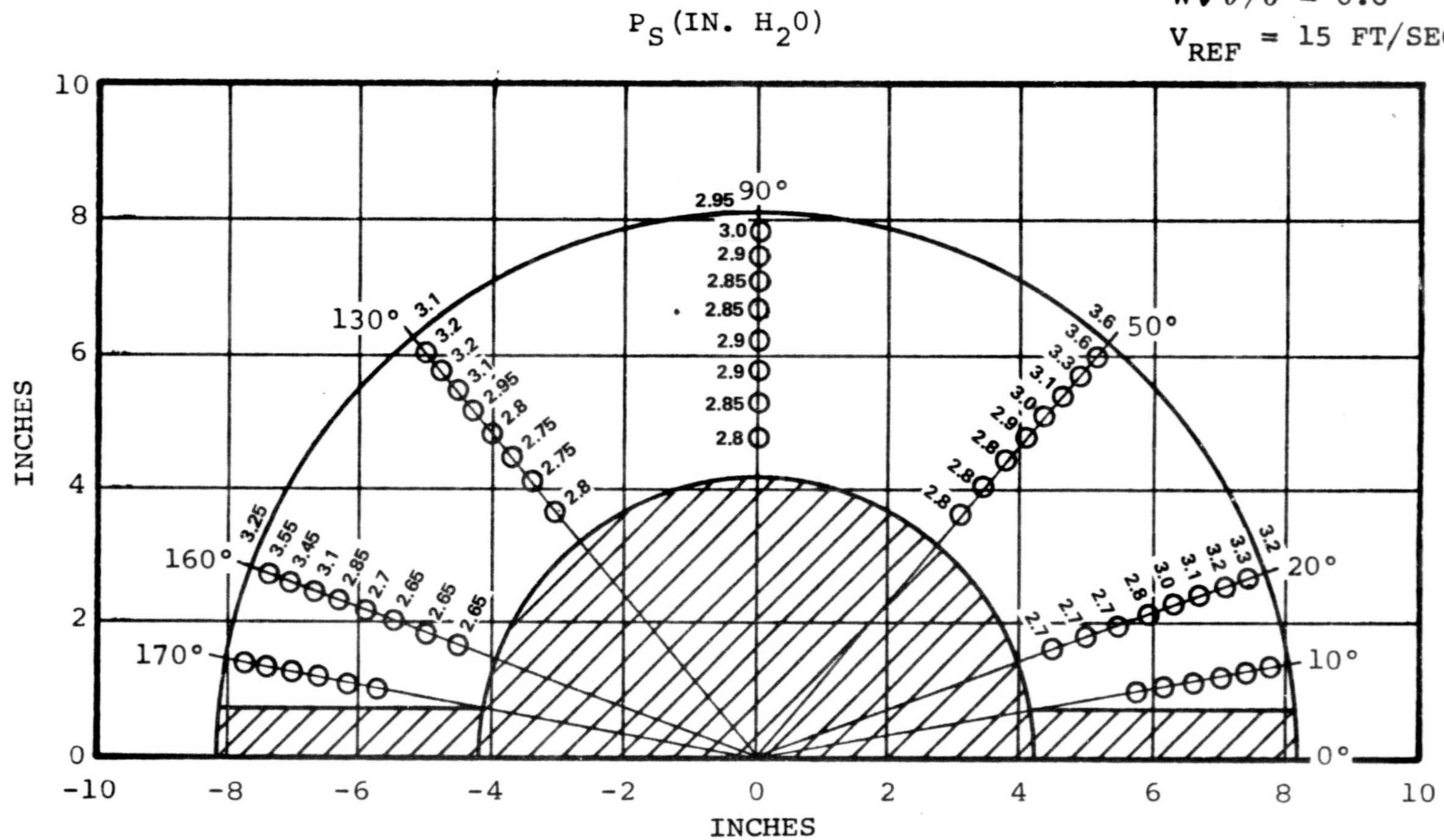

Figure 2-14. AGT LP Regenerator Cold Flow Rig.
3- WIRE SURVEY PLANE

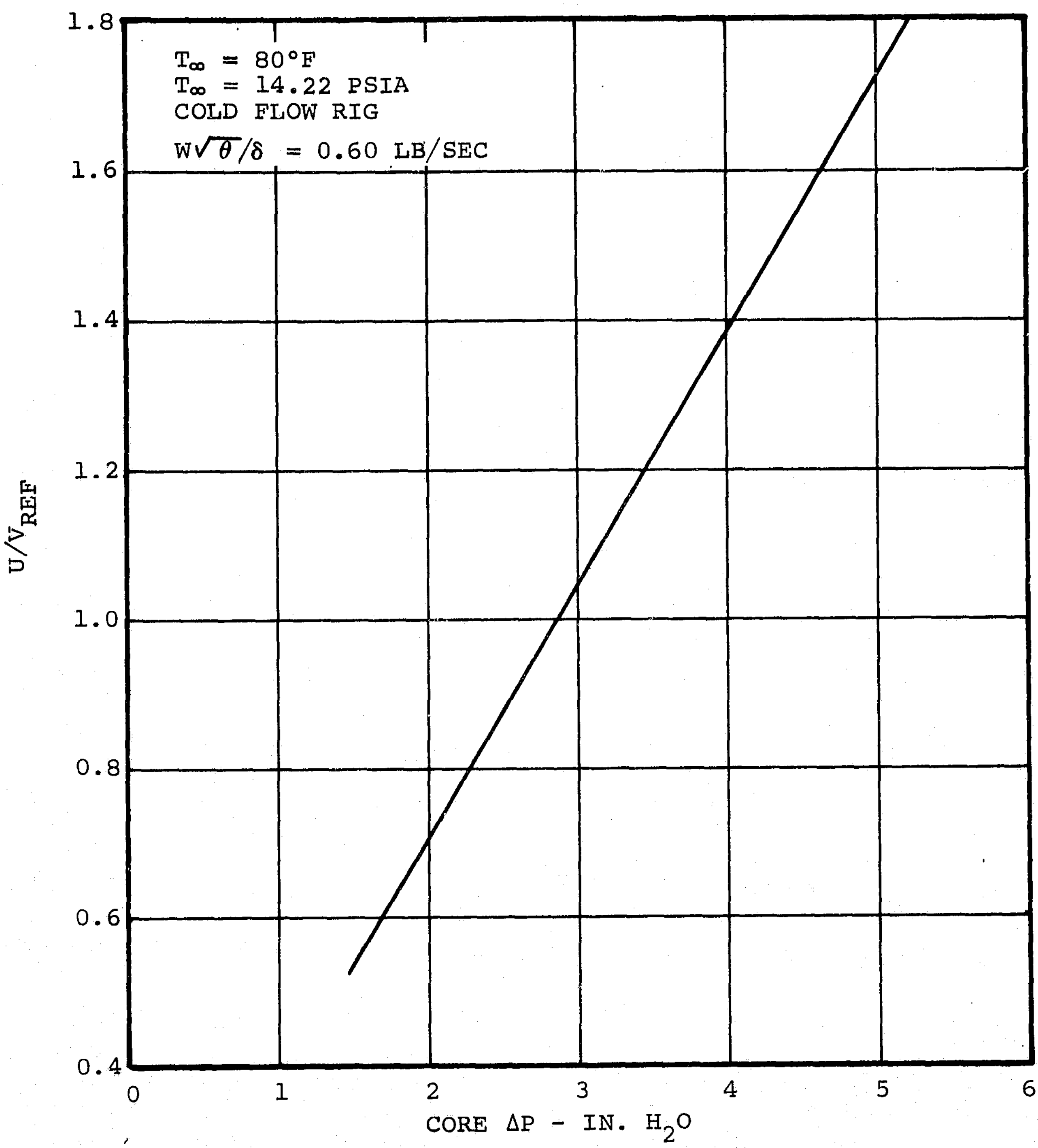

Figure 2-15. Theoretical Relationship Between Core ΔP and Velocity Ratio.

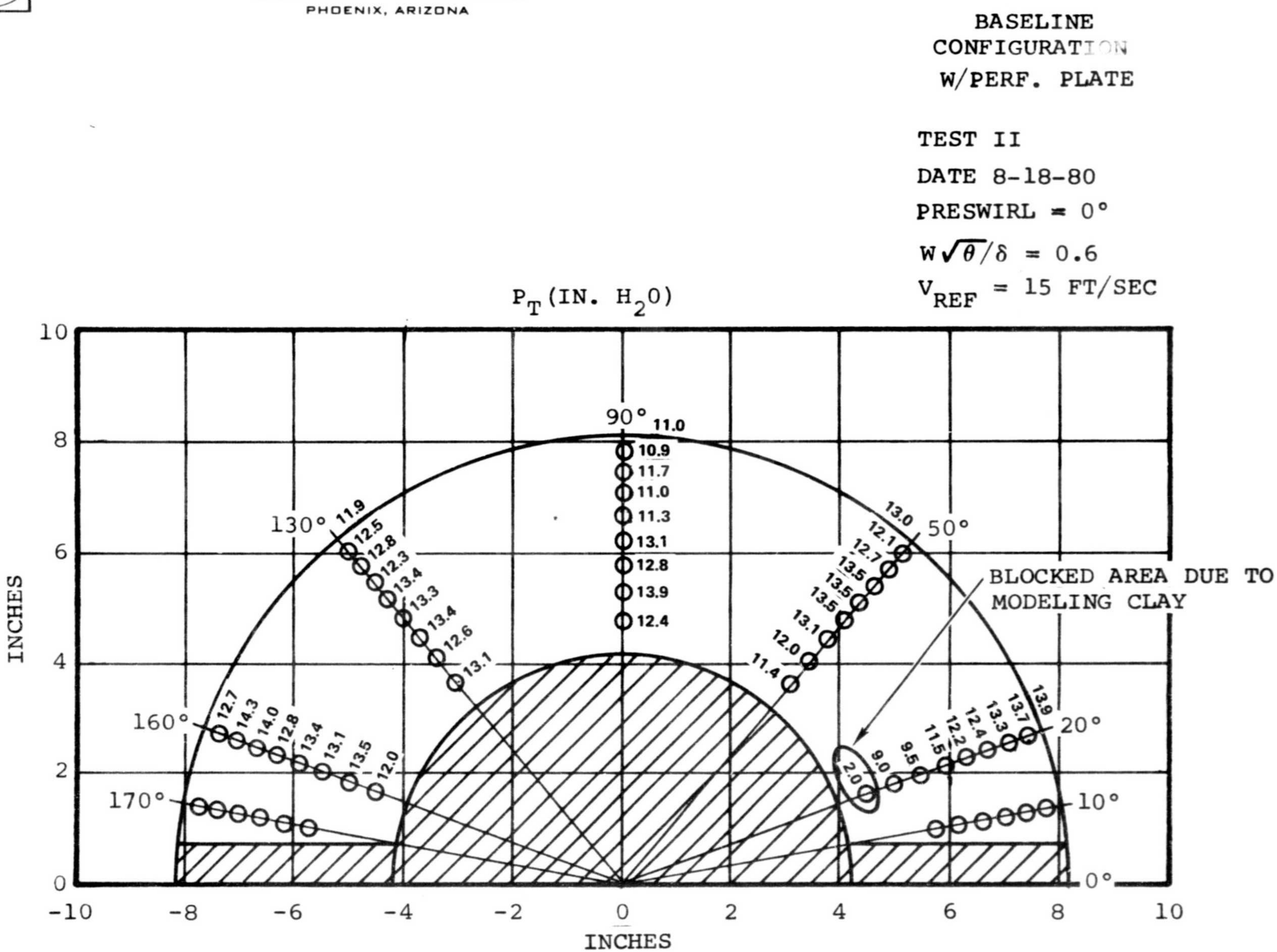

Figure 2-16. AGT LP Regenerator Cold Flow Rig
3-Wire Survey Plane.

Figure 2-17. ~16 Percent Open Area Hole Metal Plate.

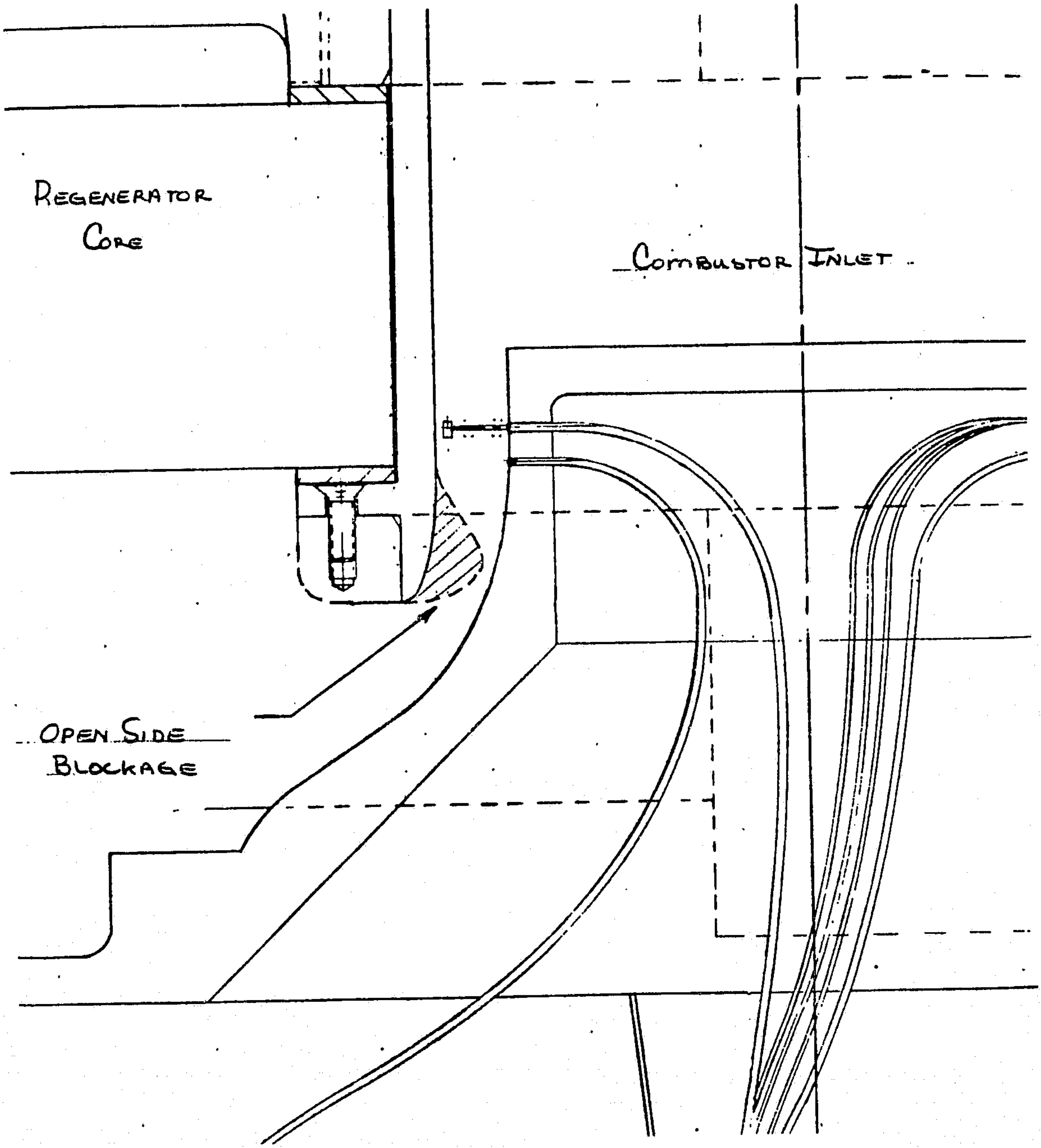

Figure 2-18. Combustor Inlet Guide Vane.

2.2.4.2 Regenerator HP Cold Rig

The combustor inlet flow distortion was evaluated in order to obtain the desired combustor inlet guide vane configuration that would minimize the combustor inlet circumferential distortion. Nineteen configurations were evaluated in terms of flow ratio (ratio of flow from the open side to the blocked side), circumferential static pressure variation at the burner inlet, and $\Delta P/P$ from the regenerator exit to the burner inlet (Figure 2-19).

Preliminary conclusions:

- None of the anticipated combustor inlet guide vane configurations [Appendix I, Page 2, Document 31-3480(09] were found to be suitable. Several iterations were therefore tested using modeling clay to produce variations in the open side area which in affect increased the $\Delta P/P$ locally and forced the flow to the closed side.

  Several shapes are currently being fabricated from aluminum in which geometry variations can be more closely controlled. Further testing of these configurations will be initiated as the hardware is received.

- Initial core survey testing is in progress. Results will be available in the next reporting period.

2.2.4.3 Regenerator Performance Hot Rig

Instrumentation requirements have been defined and conceptual design layouts initiated.

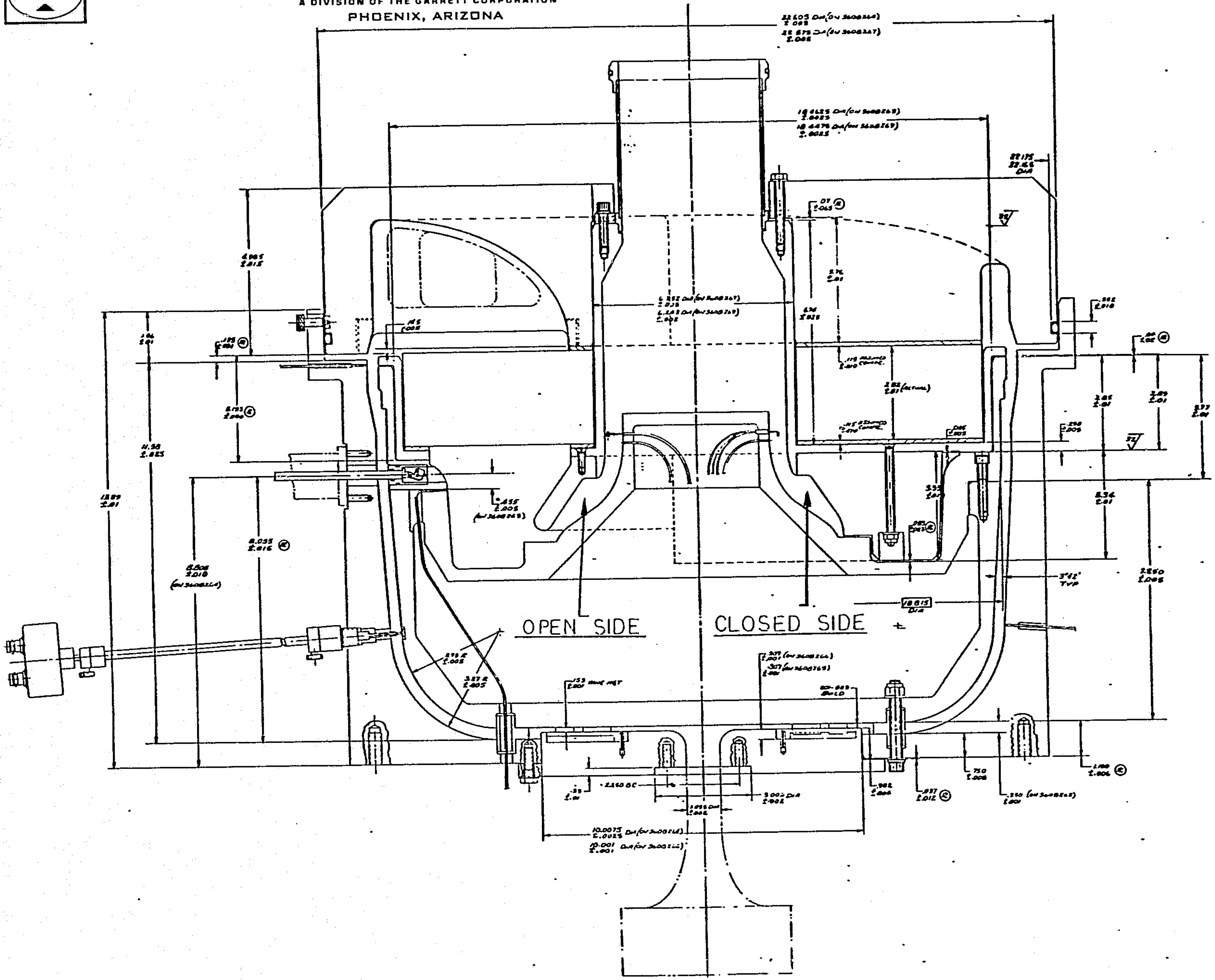

Figure 2-19. Burner Inlet Circumferential Static Pressure Variation.

Rig design relies heavily on Mod I Build 1 housings with modifications to engine seal locations, inlet ducting and exhaust ducting.

Test plan outlines for the performance and durability hot rig are being reviewed.

2.2.4.4 <u>Regenerator - Ford</u>

The inner seal crossarms for the AGT engine have been sprayed with I-112 coating at Alloy Tek. All of the regenerator seal shoes for the October 1980 delivery have now been coated. Diaphragms for the seal assemblies will be available during the early part of September 1980.

Special spacers, which simulate operating clearances for the seals in the Mod I, Build I engine, were received for the static seal rig. Seal assemblies required for October 1980 delivery will be evaluated in this rig prior to shipment.

The first NGK regenerator core was received on schedule. The core bonding fixture will be shipped the first week in September 1980. Ring gears are expected about mid-September. The first core assembly should be completed on schedule.

Debugging of the revised "core position" analysis is continuing. Analysis of the transient stress in the regenerator matrix for a cold start condition with zero core rotation for the initial 10 seconds was initiated. In order to accomplish this task the "matrix temperature distribution" program must be revised to accommodate a zero core rotation condition. The revision of this program has been initiated.

2.2.5 Gearbox/Variable Stator Torque Converter (VSTC)

2.2.5.1 Gearbox

AGT gearbox detailing continues with 83 drawings completed and submitted for checking. Of these, 16 bearing drawings have been released to date and the bearings have all been placed on order. Additionally, 16 of these details have been released for procurement. Casting details of the four gearbox housings are nearing completion and inquiries are being made to obtain low cost sand castings from various casting vendors. This action is being taken to permit gearbox design assembly and check-out prior to committing to expensive tooling. A total of 90 detail drawings are required to complete the gearbox design.

Integration of the Ford VSTC design and AGT gearbox is continuing.

2.2.5.2 Variable Stator Torque Converter (VSTC)

Fabrication and rework of the Ford VSTC (P/N 0225) test rig shaft and lever arm system have been completed except for final braze and heat treating of the twenty crank/blade elements. Upon completion of this task, the unit will be rebuilt for additional testing and to establish control response rates required for the AGT101 torque converter.

AGT Mod I VSTC detailing has been completed by Ford, with all details submitted for checking. Various assembly drawings such as the turbine, impeller, and variable stators have been distributed to vendors for bidding activity. The original vendor for the variable stator blades has been located, and blade tooling was found to be readily available.

VSTC design has been slightly modified to incorporate a stator support shaft overrunning clutch. This design feature will reduce VSTC losses during AGT idle operation.

2.2.5.3 Slave Gearbox

Slave gearbox fabrication is progressing on schedule, with the exception of the longer lead-time gearing. Detailing of the case necessary to adapt the slave gearbox and engine into an assembly has been completed and submitted for checking. This assembly is intended to permit engine component development.

2.2.5.4 Regenerator Drive Gearbox

The mounting bracket for the regenerator gearbox has been completely detailed and submitted for checking. A gearbox assembly drawing is progressing.

2.2.5.5 Automatic Overdrive (AOD) Transmission

A standard AOD transmission has been received from Ford production for setup and test to establish shift dynamic characteristics. Installation design has been completed and all necessary parts are being procured. The unit will be powered by a 15 hp vari-drive capable of attaining maximum AOD input speed. The valve body will be instrumented to monitor oil pressures at four different clutch control passage. This will provide specialized information necessary to assure compatibility of the AOD and AGT control logic. Coordination with Ford on this matter is continuing.

2.2.5.6 Transmission - Ford

Detailing on the VSTC is 85-percent complete and several discussions have been held with Davis Tool, Taylor, Mich., the fabrication source. Davis Tool makes both prototype and production torque converter assemblies for the auto industry. A firm quote on prototype costs should be available from Davis Tool, early in September. Contact with an alternate prototype source, Delta Research, Livonia, Michigan, has been initiated.

2.2.6 Ceramic Component Development

Screening test rigs for the regenerator shield, combustor baffle, transition duct, turbine backshroud and turbine shroud have been placed on order. Delivery is expected in September 1980.

Silicon Nitride shafts for turbine attachment testing have been received from ACC. These shafts will be machined to provide five interference fits (4.5, 6.0, 6.5, 7.0, and 7.5 Mil diametral) with the Incoloy 903 sleeves (P/N 3608447-1). After assembly, each shaft will be forced through the sleeve using a Riehle compression testing machine. Loads will be recorded in order to calculate the coefficient of friction for each case. The friction coefficient at room temperature will be defined without a soak, and after a soak at 1100°F. The coefficient of friction will also be determined at 1100°F.

After analysis to define the attachment interference to be used in the engine, sleeves will be applied to both ends of a ceramic shaft and tensile forces will be applied to determine separation forces at room temperature and at 1100°F.

2.2.6.1 Ceramic Material Evaluation

2.2.6.1.1 ACC Baseline Materials

Preliminary stress rupture results have been obtained for eight heat treated RBN104 test bars. These bars were heat treated for two hours in an oxidizing atmosphere at 2500°F, then were tested simultaneously in a gas-fired atmosphere at 2500°F for 300 hours. Bars were loaded in bending at 16 ksi for the initial 150 hours, then loaded to 20 ksi for the remaining 150 hours. No test bar failures occurred during the testing sequence. The test bars are currently being evaluated for weight change, and will subsequently be evaluated in four point flexure.

Stress rupture testing of baseline SNN522 has also continued. All testing is being performed on as-sintered test material in static furnace conditions. A summary of current results are presented in Table 2-3. As noted in this table, the SNN test bars loaded to 31.5 and 39.7 ksi at 2000°F exhibited strengths of 84.7 and 80.7 ksi when flexure tested at 2000°F. These flexure strength values exceed all but one flexure strength value obtained on 30 as-sintered test bars during 2000°F baseline evaluations. These post stress rupture results suggest that a strengthening effect occurred during the stress rupture exposures.

Results in Table 2-3 also indicate that bars loaded to 49.1 ksi at 2000°F exhibited a creep deflection of .003 and .005 inches when measured from the outer span load points (0.75 inch span).

Stress rupture testing at 2100°F is currently in progress and results will be presented in the next progress report.

2.2.6.1.2 Carborundum Baseline Materials

During the current reporting period the initial baseline strength testing was completed on the second group of 300 cold-pressed test bars (fine grain material) and on a group of slip-cast test bars. Weibull plots are shown in Figures 2-20 and 2-21, and data are summarized in Table 2-4. Fine grain strength of the cold-pressed material was about 5-percent greater than that obtained previously on cold-pressed material having exaggerated grain growth.

TABLE 2-3. SUMMARY OF STRESS RUPTURE RESULTS FOR ACC SNN522

Specimen S/N	Temperature °F	Stress ksi	Time hrs	Results
7949	2000	31.5	325	No failure. Flexure tested at 2000°F, failed at 84.7 ksi*
8233	2000	39.7	336	No failure. Flexure tested at 2000°F, failed at 80.7 ksi*
8012	2000	49.1	4 min.	Fractured at large inclusion
8112	2000	49.1	336	No Failure. Creep of .003" deflection
8072	2000	49.1	333	No failure. Creep of .005" deflection
8133	2100	39.7	338	No failure. Creep observed
8173	2100	39.7	120	Test in progress

*NOTE: Baseline flexure strength valves ranged from 48.2 to 80.7 ksi with a characteristic value of 66.1

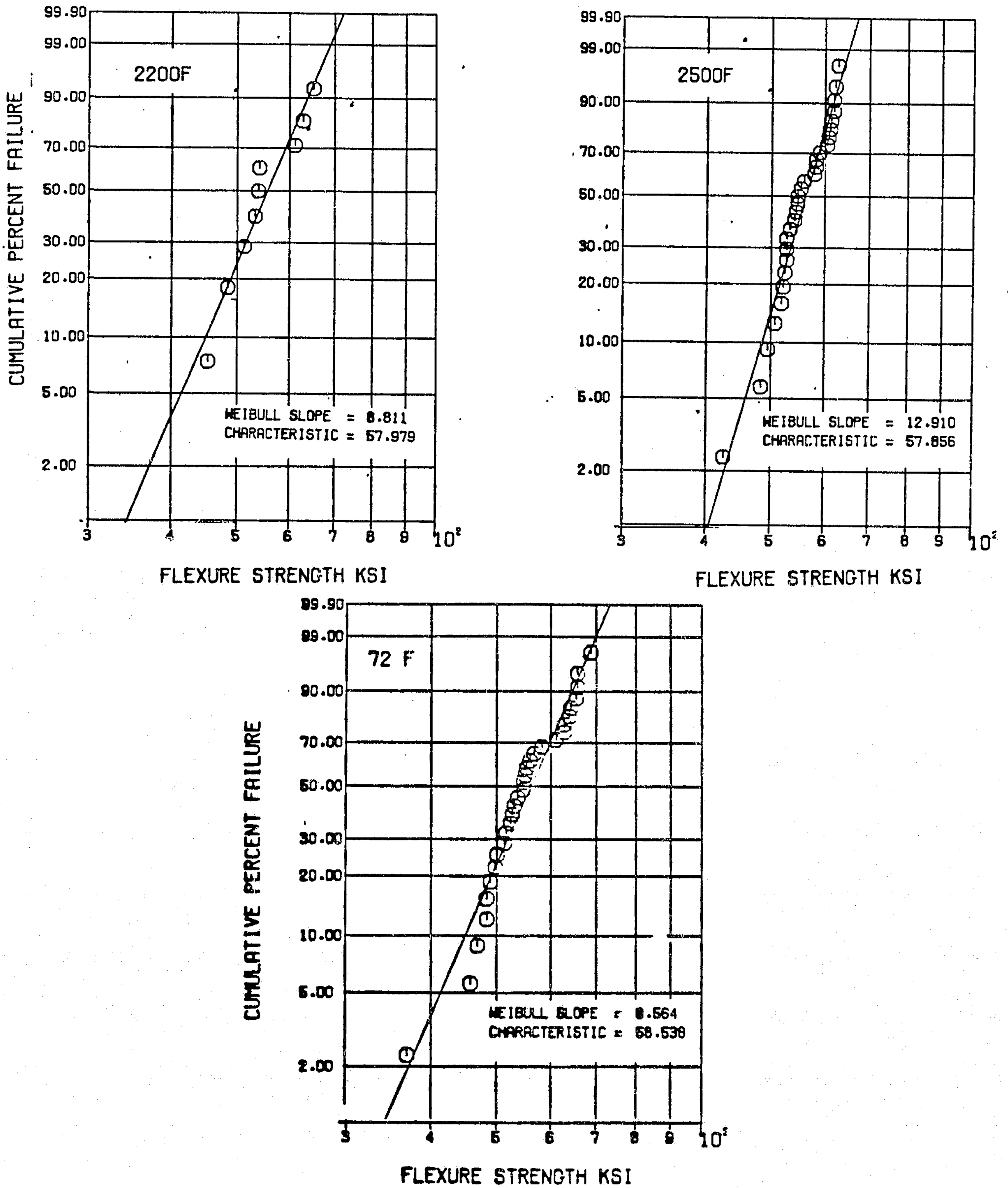

Figure 2-20. Weibull Plots for Cold-Pressed SASC at Various Temperatures (Fine Grain Material).

ORIGINAL PAGE IS
OF POOR QUALITY

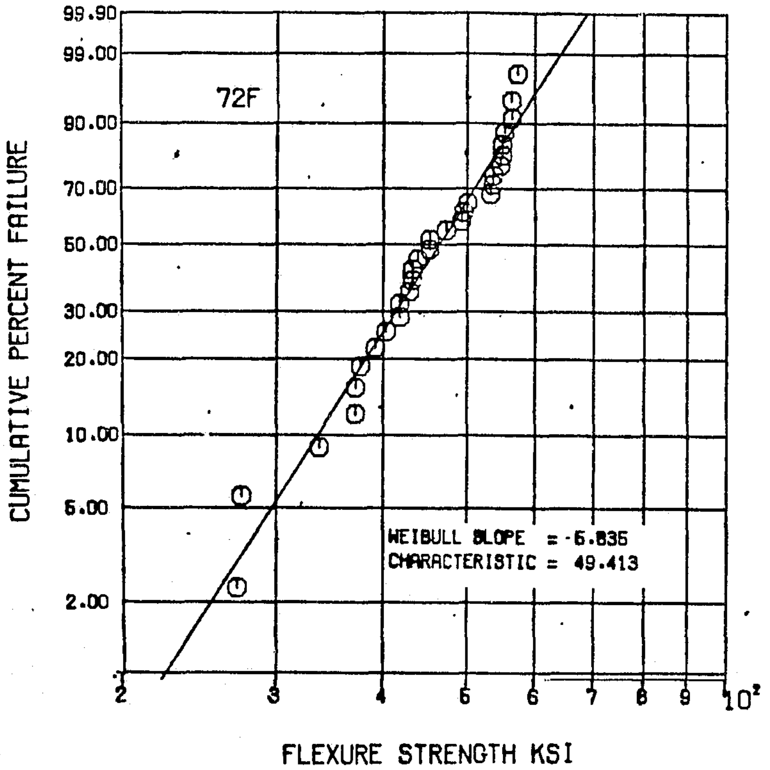

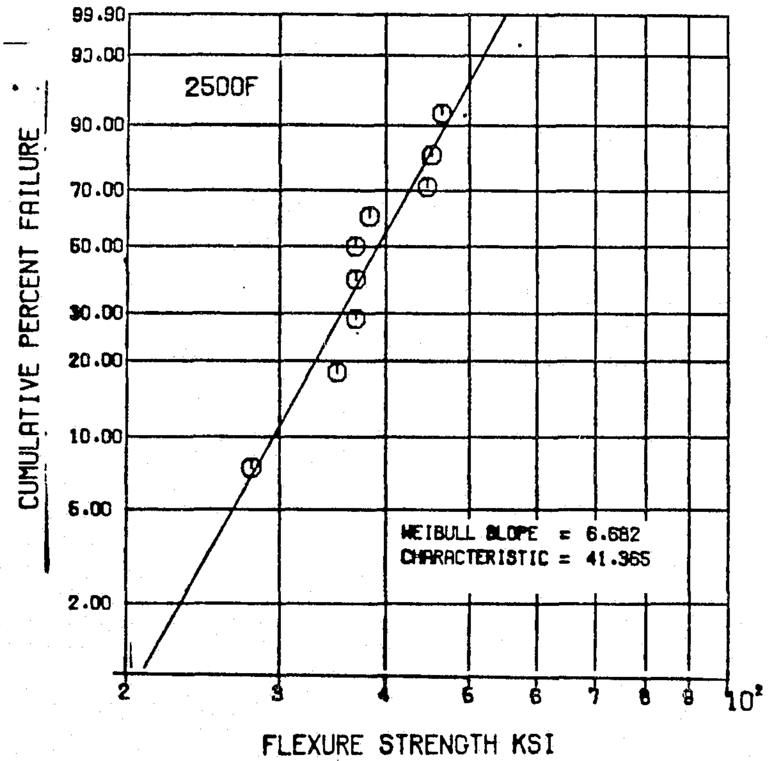

Figure 2-21. Weibull Plots for Slip-Cast SASC.

TABLE 2-4. WEIBULL PARAMETERS OBTAINED FROM FLEXURAL TESTS ON AS-RECEIVED SASC

Material (population)	Temperature (°F)	Characteristic Strength (ksi)	m-Value
Cold-pressed II* (30)	72	58.5	8.6
Cold-pressed II (10)	2200	58.0	8.8
Cold-pressed II (29)	2500	57.9	12.9
Cold-pressed II** (30)	72	59.5	8.4
Slip-cast*** (30)	72	49.4	5.8
Slip-cast (10)	2500	41.4	6.7

*Fine grain material
**Oxidized 2500°F, 4 hr
***Bimodal Casting Mix

The strength of the slip-cast test bars is lower than anticipated but is representative of the bimodal particle size casting mix currently being used for slip-cast components. Bimodal casting mix has the advantages of higher casting rates, better green strength, and lower shrinkage which should result in better dimensional control of large components. However, the disadvantages are lower density and lower strength.

Included in Table 2-4 are data on a group of cold-pressed test bars which had been oxidized for 4 hours at 2500°F prior to testing at room temperature. Previous data have demonstrated the effectiveness of oxidation treatments in healing machining damage. Since components will be given an oxidation treatment prior to use, it seemed appropriate to determine the effect of oxidation on the properties of as-received test bars. As indicated in Table 2-4 and Figure 2-22, the oxidation treatment resulted in a minimal improvement in strength. Therefore, measurements on un-oxidized test bars are representative of the component materials.

Under the common effort, Carborundum is also determining the baseline Weibull parameters of various forms of sintered αSiC. These data are also being analyzed by the AiResearch Weibull computer program to determine if any analytical differences exist and to provide a common basis for material property evaluation. (The comparison is shown in Table 2-5.) A previous comparison was contained in the Ninth Monthly Progress Report [31-3480(9)].

2.2.6.2 Subcontractor Ceramic Development

2.2.6.2.1 Ford

The Ford monthly report is included as Appendix I.

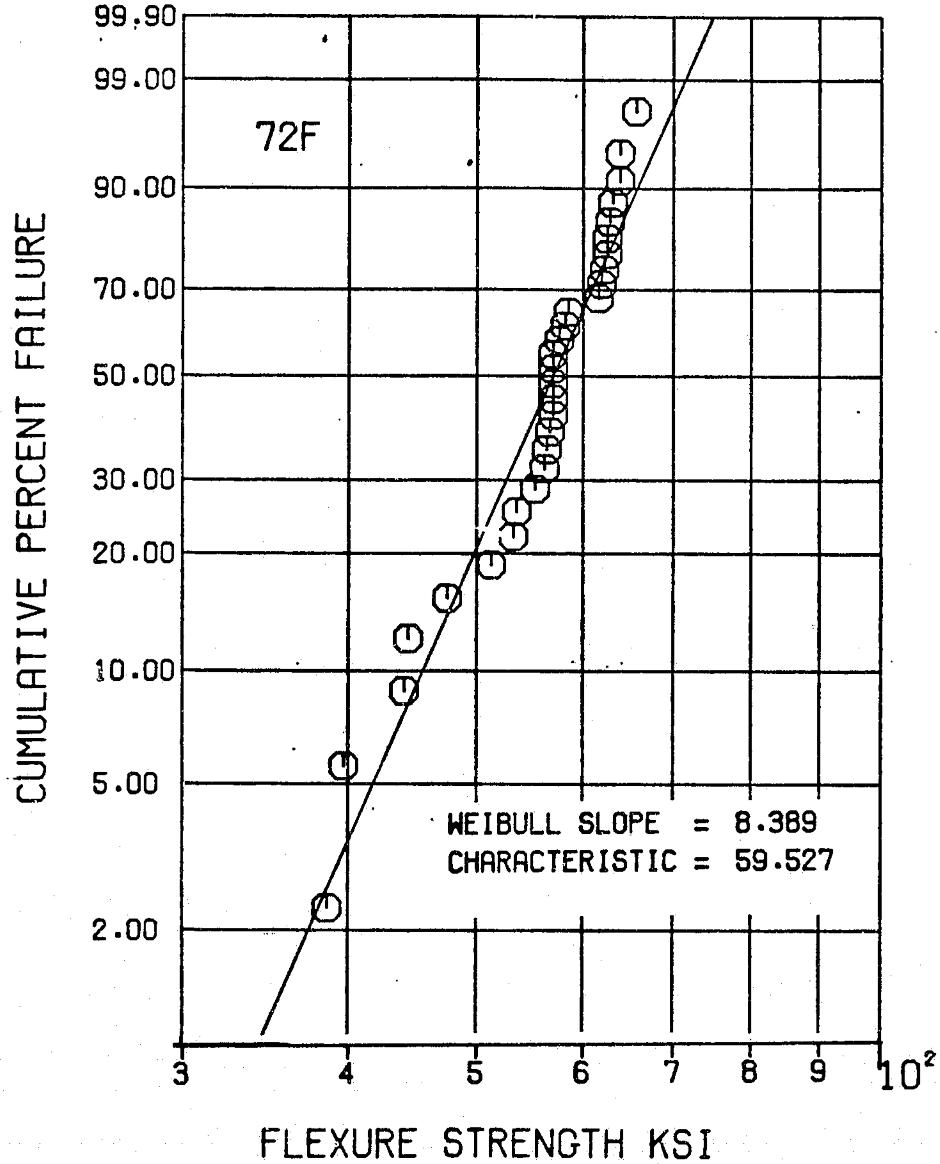

Figure 2-22. Weibull Plot for Cold-Pressed SASC After 4-Hour Oxidation in Air at 2500°F.

TABLE 2-5. COMPARISON OF CARBORUNDUM (CBO) AND AIRESEARCH (AIR) 2-PARAMETER WEIBULL ANALYSES OF CARBORUNDUM COMMON DATA AT 2192°F

Material (population)	Characteristic Strength (ksi) AIR/CBO	Weibull Slope AIR/CBO
Slip-cast (31)	65.2/65.4	7.1/6.7
Cold-pressed (31)	54.2/54.3	8.4/7.9

2.2.6.2.2 ACC

The ACC monthly report is included as Appendix II.

2.2.6.2.3 Carborundum

A simulated rotor has been received from Carborundum for spin test. The rotor is of two-piece construction with an injection molded shell and an isopressed core. The two sintered pieces were hot-press bonded using an extrudable mix of αSiC at the interface. No volume defects were detected by X-ray examination, and the rotor appears suitable for spin testing.

Carborundum monthly reports for common and unique tasks are included as Appendices III and IV respectively.

2.2.6.3 Ceramic Interface Evaluation

Studies of the sensitivity of AGT101 candidate materials to contact loading and simultaneous relative movement are continuing. However, during this reporting period a complete evaluation of the contact stress apparatus calibration and set up procedures was performed. This procedure review was initiated when inconsistant coefficient of friction results were obtained during the initial AGT studies. The review included both analytical and experimental confirmation of pneumatic cylinder loads vs normal forces between ceramic specimens (see Figure 2-25); Instron load cell output vs sliding forces at the ceramic interfaces; the influence of vertical alignment of the load bar pivot and the ceramic specimen interface on coefficient of friction measurements; and the influence of pneumatic cylinder loads on Instron load cell output.

Completion of this study resulted in the replacement of the spring return pneumatic cylinder with a low friction diaphram air

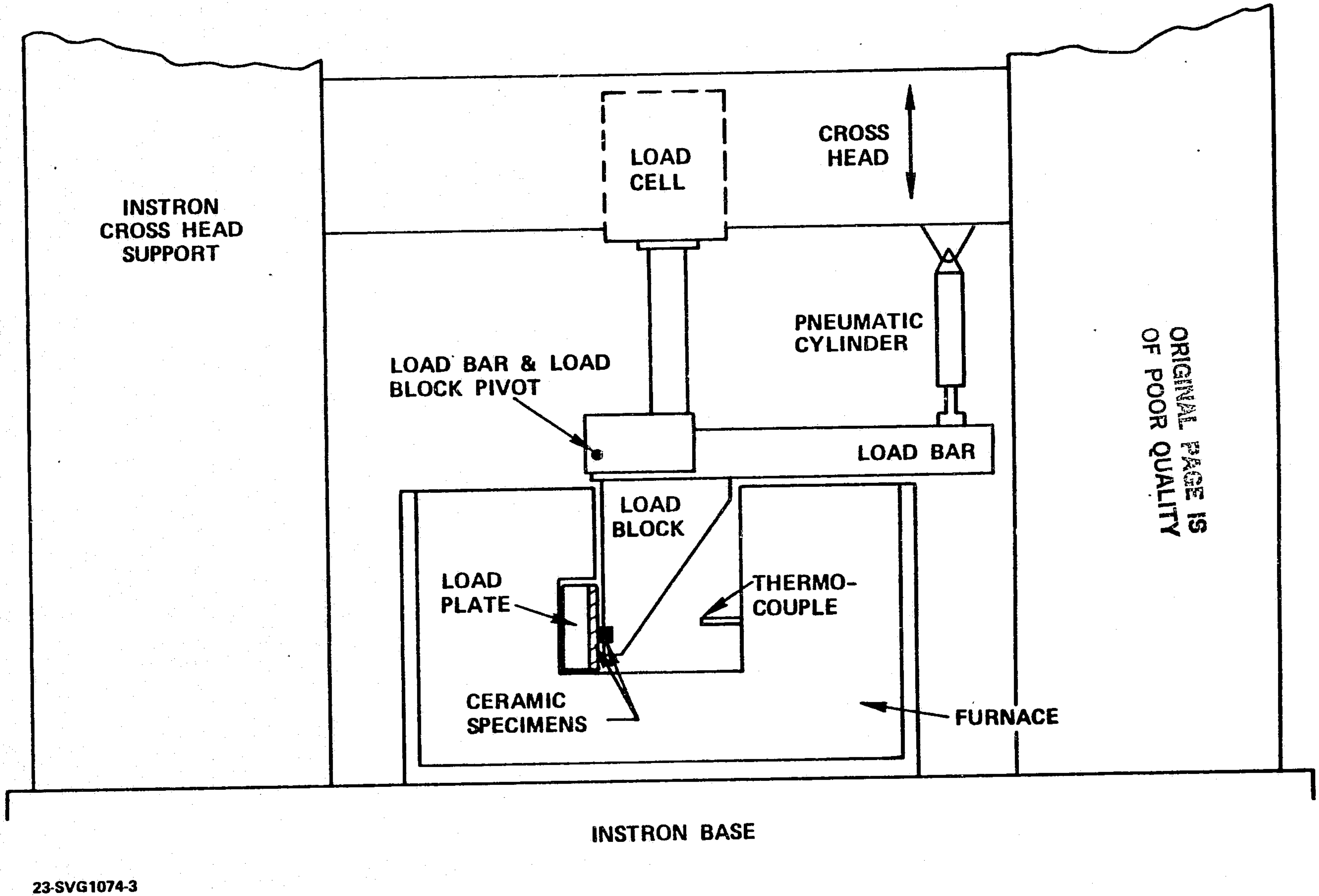

Figure 2-25. Interface Test Apparatus.

cylinder for reproducible normal force application, and the use of a set-up procedure to assure load bar pivot vertical alignment with the ceramic specimen interface.

Ceramic interface studies have resumed with the establishment of coefficient of friction vs normal force and temperature baseline data for Carborundum sintered α-SiC. Subsequent studies will include the establishment of ACC RBN104 baseline data, and the evaluation of ceramic coatings.

2.2.7 Foil Bearing

2.2.7.1 Single Foil Bearing Test Rig

Development testing of the single foil bearing test rig is continuing. Bearing designs evaluated include foils with backing springs and foils without backing springs. The foil and spring designs have been varied to establish a family of bearing configurations that can be selected for subsequent testing and development in the rotor dynamics test rig and AGT101 engine. The following is a list of foil bearing tests conducted:

- Static spring rate
- Dynamic spring rate
- Stability
- Load
- Power loss
- Lift-off and roll down

The basic foil bearing configuration selected for rig testing is as follows:

Basic Bearing Configuration

Number of foils and springs	7
Thickness of foils	0.005 inch
Foil arc length	1.220 inch
Foil axial length	1.075 inch
Foil preformed radius	0.850 inch
Spring "X" dimension and axial length	0.003 inch X 0.585 inch
Spring performed radius	0.700 inch
Sway space	0.010 inch

Eight foil bearing configurations were assembled and tested, of which, seven had variations from the basic configuration. These can be seen in the following chart:

Configurations Tested

Configuration No.	Major Variation From Basic
1	Basic
1B	Foil length 1.190 inch
2	"X" dimension = 0.0052 inch
3	"X" dimension = 0.0062 inch
3B	Configuration 3 + foil length 1.190 inch
4	"X" dimension = 0.0052 inch Spring radius = 0.675 inch
4B	Configuration 4 + foil length 1.190 inch
5	No backing spring

Foil bearing configuration numbers 1B, 3B and 4B all exhibited adequate performance characteristics as tested, permitting any of these bearings to be considered usable in the Mod I, Build 1 engine configuration. Figure 2-26 shows a comparison of load versus power loss for the three bearing configurations. Other promising configurations will be tested during the next reporting period.

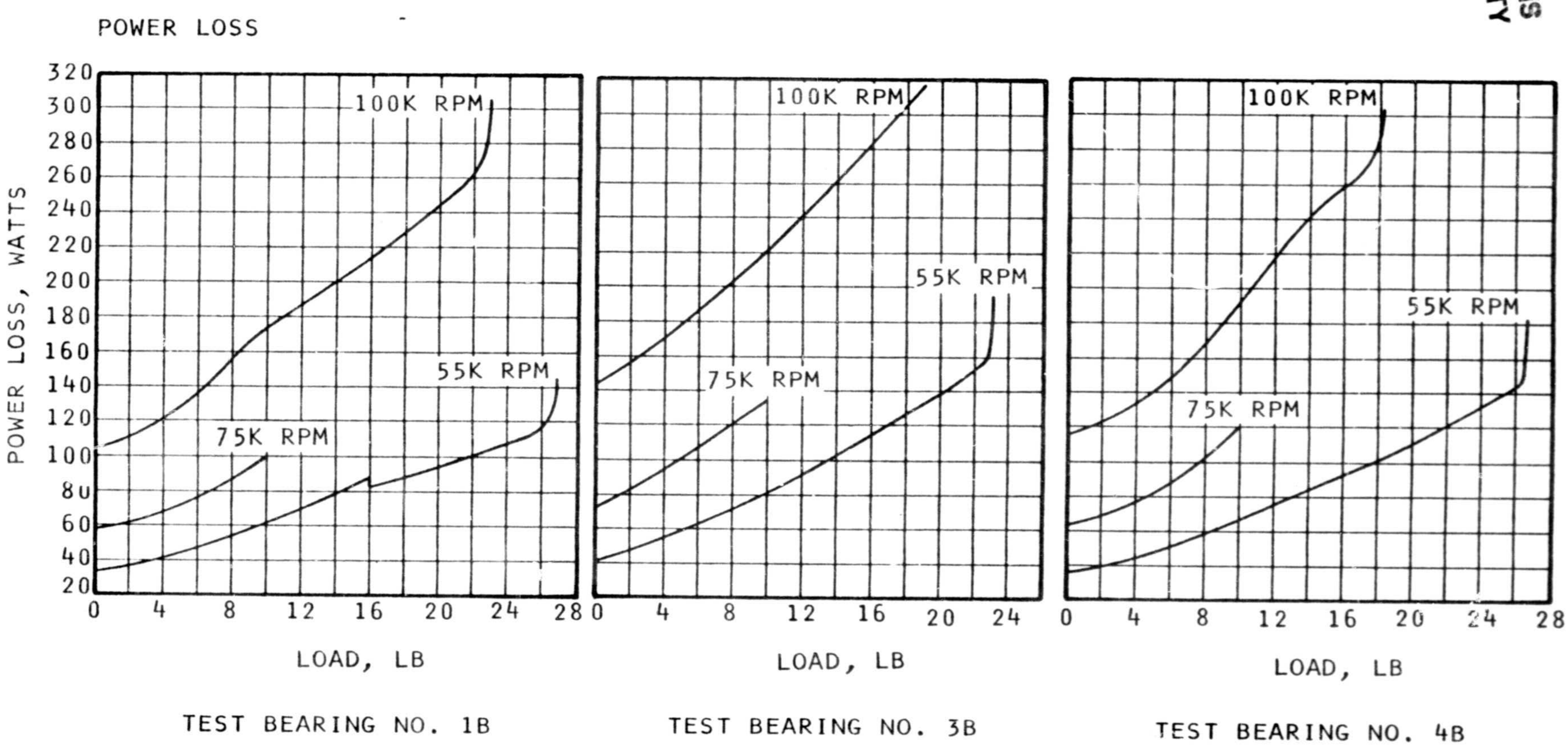

Figure 2-26. Bearing Configuration Load Versus Power Loss.

2.2.7.2 Dynamic Foil Bearing Test Rig

Detailing of the Dynamic Foil Bearing Test Rig has been completed and all component hardware has been placed on order, test cell preparation for the rig has been initiated.

2.2.8 Seals

Detail drawings of the high speed ring seals have been completed and all parts have been placed on order for the Mod I and Mod II engine configurations. The Mod II engine seal will include wave springs to preload the seal rings whereas the seal for the Mod I engine will not include wave springs due to the higher buffer air pressure introduced into the seal for cooling purposes. Severe engine space limitations require a modular seal design for both the Mod I and Mod II configurations.

A separate seal design with replaceable components has been completed for use in the seal test rig. All parts have been placed on order. The functional rings and stators of the replaceable component seals will be identical to the components used in the modular seals.

2.2.9 Rotor Dynamics

Components fabrication for the rotor dynamics test rig is proceeding on schedule. The test cell for the rotor dynamics and foil bearing test rigs will be adapted from and existing test chamber. A remote control panel and connection to the computer data acquisition system will be included.

2.2.10 Controls

Fuel System

Evaluation test of the Bosch automotive injector has been completed and documented. An injector from a Lincoln provides the best linearity of the various units tested when operated at 15 Hertz and 10 psid.

Electronic Control

Software for the input signal monitoring and mulitplexing has been completed. The output software is now in process.

Electrical Accessories

The high temperature thermocouple drawings have been released. Location and configuration of the eddy current speed sensor is still pending.

The starting/charging circuit has been tentatively defined using commercially available contractors to effect the 24-volt starting and 12-volt charging configuration.

Mechanical Accessories

A scheme for anticipating transmission shifting by monitoring selected pressures within the transmission has been defined. The Ford AOD transmission will be installed in the laboratory to evaluate shifting. This test will provide insight into the feasibility of anticipating shifts, if required, to reduce geartrain stresses during shifting.

2.3 Task 3.0 Experimental Powertrain Development

Power Section drawing refinement continues for the Mod I, Build 1, AGT101 powertrain. Detail drawings for all of the cast housings have been started. Liaison work on these castings has been conducted and vendor inputs have been integrated into the drawings which should be completed in early September. This delay in drawing completion will not impact the critical milestone schedule.

2.4 Task 4.0

No activity for this reporting period.

2.5 Task 5.0 Vehicle Integration - Ford

Work continues on the vehicle climate control system required to adapt the AGT101 engine to the Ford Fairmont.

Preparation of a AGT101 Engine/Vehicle Acceptance Specification is in progress.

2.6 Task 6.0 - Manufacturing, Cost, and Marketability Study

No activity for this reporting period.

2.7 Task 7.0 - Program Management

The monthly AGT101 program review was held in Phoenix on August 19-20, 1980. Considerable discussion was held concerning the FY81 funding limitation. AiResearch agreed to perform a cost estimate of the FY81 effort to determine what effort could be deferred or deleted to accommodate a funding limitation less than the projected expenditure level. Extraordinary inflation is the primary cause of the cost growth.

On August 9 and 11, 1980 AiResearch particpated in the Auto Energy Days exhibition at Ames and Council Bluffs, Iowa. The exhibition was sponsored by Representative Tom Harkin of Iowa, Chairman of the House subcommittee on transportation. The AGT101 mock-ups and displays were set up; explanations to the congressman, press and public were provided by Mr. Ed Strain of AiResearch.

2.8 Task 8.0 - Reporting

Figure 2-27 presents the 1980 AGT101 Program reporting schedule. In addition to reports shown in this schedule, all presentation material is also documented and furnished to DOE/NASA. Aside from the monthly progress reports, the major documentation task completed during the reporting period was the submission to NASA of the Semi-Annual Technical Summary. This report summarized the technical accomplishments of the AGT program from the inception of the program to June 30, 1980.

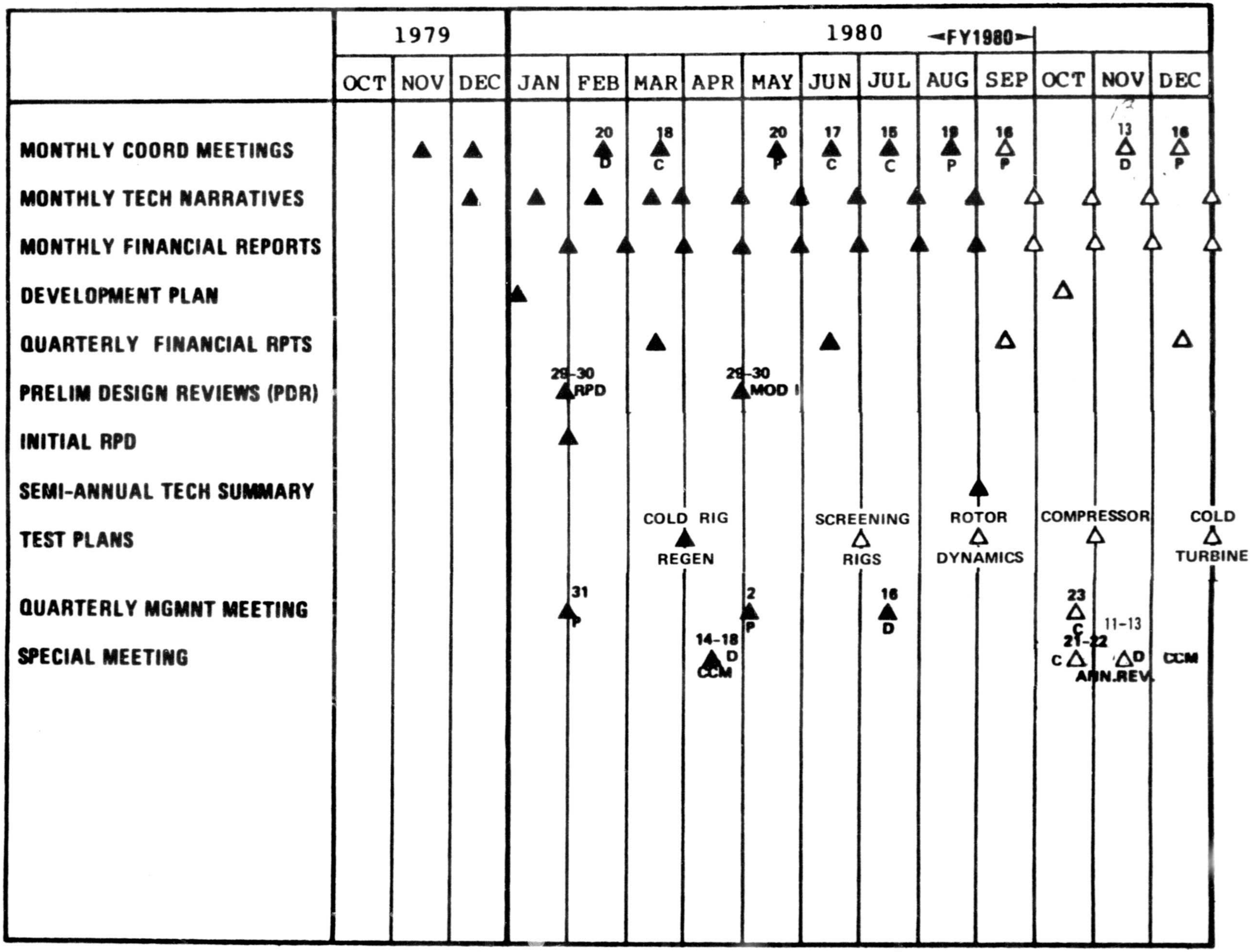

Figure 2-27. AGT101 1980 Reporting Schedule.

APPENDIX I

FORD AUGUST PROGRESS REPORT

(2 pages)

APPENDIX I
FORD AUGUST PROGRESS REPORT

1. CERAMIC ROTOR - FORD

Slip Casting

Nine simulated rotors were cast this month. After mold removal, five parts looked good, with no observable cracks. Two parts may have small cracks, while the other two have large cracks. Cracking appears worse when high humidity conditions prevailed, resulting in slow casting rates. Additional mold drying appears to alleviate the problem.

Nitriding

Nitriding runs continue to use the full demand cycle, resulting in long runs when nitriding simulated rotors. Five simulated rotors were nitrided in each of two runs. Results of the first run were three good simulated rotors with good weight gain, two cracked rotors with low weight gain. The second run was just completed, and has not been analyzed as yet.

Sintering

Only one sintering run was produced at the vendor, due to mechanical problems plus in-house commitments by the vendor, creating a problem concerning staying on schedule. After discussion with the vendor, the problem appears solved. The next sintering run is expected during the first week in September.

The Ford sintering furnace was received and installed. During start-up trials by the vendor's field engineer, the microprocessor-based control system malfunctioned. This has been returned to

Research Inc. for repairs, causing a delay of probably one month in bringing our furnace up to operational status.

Material Evaluation

Oxidation testing of the 8-percent Y_2O_3-Si_3N_4 sintered material was continued, but no reportable data has been obtained.

2.0 CERAMIC STRUCTURES - FORD

Stator

A group of test bars were molded of the 2.7g/c.c. RBSN stator material. The test bar tool, procured for this program, was found to be deficient in several aspects and is presently being reworked. The bars were processed through binder burnout, and will be nitrided next month, but may be of questionable quality.

Housing

Corning has supplied a work plan covering the period from August 15, 1980 through February of 1981. Work is presently in progress to construct a wooden model and to design patterns. Delivery of the first housing is expected sometime between January and late March, 1981, with consequent deliveries to be at the rate of one housing per month.

A static pressure test fixture to be used to proof test housings after firing but before extensive machining, was designed at Ford. Detailing is over 50-percent complete.

APPENDIX II

ACC CERAMIC DEVELOPMENT

APPENDIX II

ACC CERAMIC DEVELOPMENT

I. TECHNICAL PROGRESS

BCDA Rotor - Materials and Fabrication Development

Extruded Rotor

The modification of the rotor tool for use on the Mohr extruder for transfer molding was completed. After the first attempt to transfer mold a simulated rotor, it was evident that insufficient vacuum was being maintained and also that a larger quantity of material in the chamber was necessary to permit complete mold fill. Additional O-ring seals were added to the tool to correct the problem of insufficient vacuum holding capability. In addition, a plate with an O-ring seal was fabricated to seal off the open end of the extruder. This permitted the chamber to be evacuated while the material was pressed into a billet to eliminate entrapped air. The plate was then removed and replaced by the rotor tool. After molding the tool was removed from the extruder and it could be seen that the material had a grainy appearance which looked similar to the pelletized batch prior to molding. This seemed to indicate that the time the mold was held at temperature was insufficient to fluidize the binder within the more massive portion of the rotor. Another batch was prepared and molded and left in the mold at temperature overnight. After cooling and removing from the mold, the interior of the rotor appeared the same as the previous molding. It was also found that one of the heater bands had burned out. This is now in the process of being repaired. However, this was not the probable cause inasmuch as temperature readings on the tool itself indicated that the temperature was maintained at 200°F throughout the holding period. It is suspected that loss of binder resulting from repeated use of the material batch caused a situation whereby insufficient binder remained to completely homogenize the material. An evaluation of this possibility is presently being conducted.

Injection Molded Rotor

A rotor was injected using a hollow tube sprue which extended to the top of the rotor shaft portion. After injection the sprue was removed while the material was still plastic. The rotor was left in the heated tool and additional material was injected to fill the void left by the sprue tube. After the rotor cooled it was broken apart to determine the effectiveness of knitting homogeneously . Good knitting was found and no evidence of material separation was observed. Additional rotors will be molded and the center drilled out to remove voids and then reinjected to fill the cavity.

Slip Cast Rotor

A simulated rotor was slip cast and placed in the humidity chamber still in the mold. Humidity was maintained at 75 percent overnight. The following morning the part was removed from the mold and replaced in the chamber. The temperature (dry bulb) was increased 5°F per hour and the humidity was held between 90 and 98 percent relative until the temperature was increased to 175°F. At this point the humidity was decreased to 10 percent relative and the temperature maintained at 175°F overnight (16 hours). The temperature was then reduced 10°F per hour to room temperature. Despite this carefully controlled cycle, the rotor showed evidence of hairline cracks. It would appear that, to date, vacuum drying is the most effective method of controlled drying slip cast SNN series material.

Slip Cast SNN502 Material Studies

It was suspected that the Y_2O_3 additive (as one of the sintering aids) might create difficulty in slip casting due to its reaction with water, causing hydrolysis. In an effort to tie up the sintering aids and make them less reactive with the aqueous medium, a batch of Y_2O_3 and Al_2O_3 was pre-reacted by sintering prior to addition to the Si_3N_4 batch. This work is presently being conducted and results are expected to be reported in the next monthly report.

Previous studies which involved pre-calcining the slip batch appeared promising in that plates cast from the material did not show evidence of cracking. To pursue this approach further, a batch of sufficient quantity to cast a simulated rotor was calcined at 1200°C (approximately 2200°C) for 16 hours. This material has been prepared into slip and is presently aging prior to casting.

Fabrication of slip cast shafts for attachment studies is continuing. The first five shafts submitted during this report period were unsatisfactory due to warpage which occurred in the sintering run. Shafts were made of sufficient length to machine two shafts of the desired length from each one. However, by the time the OD was machined sufficiently to remove the warp only one shaft could be obtained. A larger diameter tool is being fabricated to increase the machine stock which should allow for the 2-in-1 shaft configuration. In the meantime, other methods of supporting the shaft during sintering are also being evaluated.

BGD - Ceramic Structures

Fabrication of all ceramic structures is on hold awaiting the arrival of tooling. The stator vane tool is the longest lead time component and delivery is promised by January 12, 1981 or sooner (18 weeks). Delivery promises for the remaining tooling has not yet been obtained.

The first of a series of nitriding runs to compare the potential effect of helium addition to the standard H_2-N_2 atmosphere have been completed. Both runs contained baseline (RBN-104) test specimens and specimens prepared with different nitriding aid amounts and chemistries. This evaluation has revealed little, if any, advantage of helium to a standard nitriding run. The results are tabulated on the following page.

	H_2-N_2 MOR (KSI)	H_2-N_2-He MOR (KSI)
Baseline (RBN-104)	47.0	47.0
Nitriding Air Chemistries		
1.5% Fe_2O_3	39.7	41.7
1.5% Cr_2O_3	38.8	38.8
1.5% Fe_2O_3 + 1.5% Cr_2O_3	41.8	41.0

Also intended to be included in these runs were specimens prepared from fractions of air classified powders, however, test specimens were not prepared in time. These specimens will be included in future nitriding runs.

II. CURRENT PROBLEMS - None

III. WORK PLANNED FOR NEXT REPORTING PERIOD

1. Material and Process Development:

A. SNN Series

(1) Evaluate slip casting capability of pre-reacted sintering aid slip batch.

(2) Slip cast rotor with slip prepared from calcined powder.

B. RBN Series

(1) Initiate second in series of nitriding atmosphere and cycle comparisons.

2. Fabrication Development:

A. Rotor

(1) Inject SNN series rotor using longer holding injection pressure time.

B. Static Structures

(1) Obtain tooling delivery schedules for remaining components.

APPENDIX III

CARBORUNDUM COMMON DEVELOPMENT WORK

ADVANCED GAS TURBINE (AGT) PROGRAM

CARBORUNDUM COMMON WORK

PROGRESS REPORT NO. 8

JULY 1 THROUGH JULY 31, 1980

AUGUST 6, 1980

M. SRINIVASAN
PROJECT MANAGER

THE CARBORUNDUM COMPANY
ALPHA SILICON CARBIDE DIVISION
P.O. BOX 832
NIAGARA FALLS, NEW YORK 14302

31-3480(11)
Appendix III

This monthly report covers the activities between the period 1 through 31 July 1980.

1 - ROTOR FABRICATION

1.1 - Joining Studies

1.1.1 - Joining Cylinders

Two cylinders containing sinterable powder as the joining medium (See hot pressing effort reported in May Monthly Report) were cut into MOR bars of the cross section 0.125" x 0.25". These were tested at room temperature in 4-point bend by using 0.75" inner span and 1.5" outer span. The results are as follows:

Bond Failure (10^3 psi)		Joint Material Failure (10^3 psi)	
44.47	†	31.95	†
37.34	†	43.99	†
33.12	††	35.96	†
28.14	††	31.52	†
29.05	††	32.53	†
21.59	††		
26.75	††		

No base material (isopressed alpha SiC) failure was observed. The cylinders were preoxidized before joining. In the fabrication of cylinder D654-6, pressure was applied only when temperature was very high during hot pressing. Because of partial presintering that occurs before the application of pressure, further densification during subsequent hot pressing is not optimum which results in low strengths. Also pre-oxidized surfaces inhibit good bonding resulting in many bond failures, as observed.

---

† Bars from Cylinder D539-92.
†† Bars from Cylinder D654-6.

These strength results should be compared with earlier ones (June Monthly Report) in which bond failures averaging approximately 25,000 psi, and joint material failures averaging approximately 47,000 psi were obtained.

1.2 - Thixotropic Casting

Figure 1 is a photomicrograph of the interface area of the shaft-hub joint which was described in the June Monthly Report. The shaft, top of the picture, is centrifuged coarse-grained SiC. The hub, at bottom, is the coarse-grained SiC thixotropically cast. Although the surface of the hub was machined to provide a clean bonding area and to remove the excess resin, it still shows signs of resin concentration at the surface. During curing stages, the excess resin causes fine cracks and crazing, visible in the photograph. The fine particle size material observed between the shaft and hub is fine-grained SiC casting mix used as a cement and filler.

1.3 - Hub Alternates

In this work, submicron alpha silicon carbide was hot pressed at 1800°C (3272°F) and 2000°C (3632°F) into approximately 1.25-inch diameter disks using boron as a hot pressing aid. The disks, hot pressed at 1800°C, had densities in the range of 2.93-3.10 g/cc whereas the disks hot pressed at 2000°C had densities in the range of 3.20-3.21 g/cc. Compositional variations in boron and carbon were also allowed. MOR bars were sliced out of these disks to 0.1" x 0.07" cross section with edges chamfered. Room temperature flexural strength was measured in 3-point bend by using a span of 0.75 inch. There were no significant differences in the strength of specimens hot pressed at 1800°C and those at 2000°C. The effect of compositional variation is summarized in the following Table I.

TABLE I

EFFECT OF CHEMISTRY ON STRENGTH OF HOT PRESSED ALPHA SIC

Percent Boron	Additive Carbon	σ_f (ksi)
0.5	1.0	53.71 ± 9.11
0.5	2.0	70.01 ± 13.71
0.3	1.0	58.41 ± 11.67
0.3	2.0	50.46 ± 6.87

ORIGINAL PAGE
BLACK AND WHITE PHOTOGRAPH

FINE GRAINED SiC BOND

CENTRIFUGAL CAST SHAFT

THIXOCAST HUB

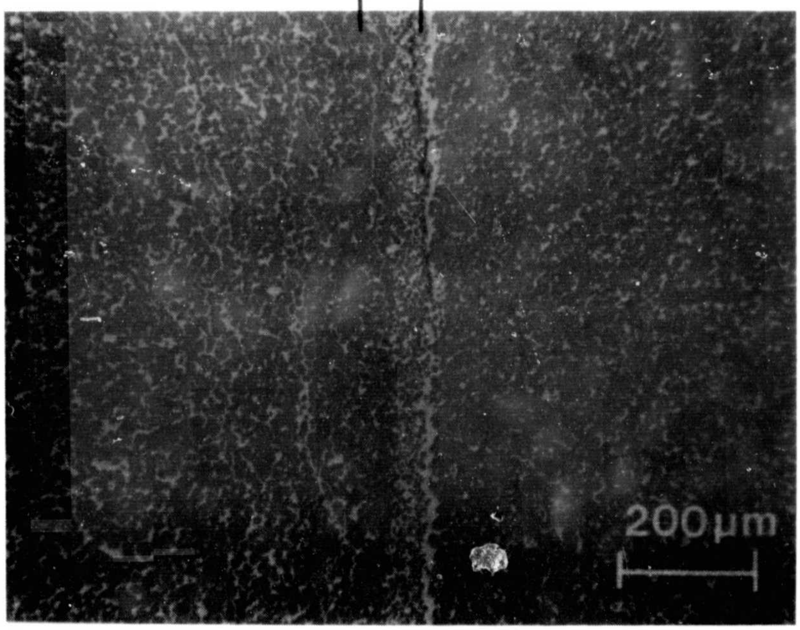

FIGURE 1: MICROSTRUCTURE OF THE HUB-SHAFT INTERFACE AREA OF RBSIC ROTOR

The microstructure of a specimen hot pressed at 2000°C and which exhibited the highest strength of 91.83 ksi is shown in Figure 2. The failure origin for this specimen appeared to be a chamfer damage under SEM investigation. The microstructure of another specimen hot pressed at 2000°C and which exhibited a low strength of 37.92 ksi is shown in Figure 3. The failure origin for this specimen was a series of several machining surface flaws adjacent to each other. The failure causing defect for another specimen (σ_f = 82.91 ksi) is shown in Figure 4 to be a poorly-bonded region below the tensile surface.

Because the strength levels achieved in this effort are considerably lower than what is needed, no further effort is planned with boron additions. However, a limited effort is underway to hot press alpha SiC with aluminum additions and to characterize the strength of the resulting material.

2 - NONDESTRUCTIVE EVALUATION

2.1 - Seeded Defect Disks

The fabrication of disks with medium size (50-125 μm) carbon inclusions were completed; as well as the disks with large size (125-250 μm) boron carbide inclusions. NDE will follow for these specimens.

2.2 - Microfocus X-Ray

Microfocus x-ray NDE was carried out with the seeded defect disks and the results are summarized below:

TABLE II

STATUS OF NDE OF SEEDED DEFECT DISKS

Thickness (inch)	Void		Carbon Inclusion		B_4C Inclusion	
	50-125 μm	125-250 μm	50-125 μm	125-250 μm	50-125 μm	125-250 μm
0.1	D	N.D	--	D	--	D
0.125	D	N.D	--	--	--	--
0.25	X	D	X	D	X	D
0.50	X	D	X	--	X	--

D = Detected
N.D = Not Detected

X = Specimen Unavailable
-- = NDE In Progress

ORIGINAL PAGE
BLACK AND WHITE PHOTOGRAPH

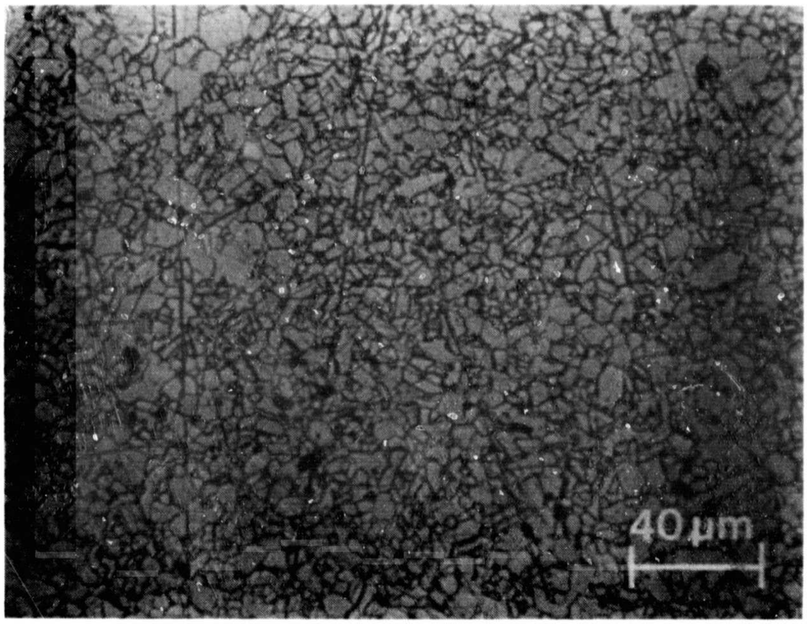

FIGURE 2: S. NO. 4-1.2. MICROSTRUCTURE OF ALPHA SILICON CARBIDE HOT PRESSED AT 2000°C

MP-74089

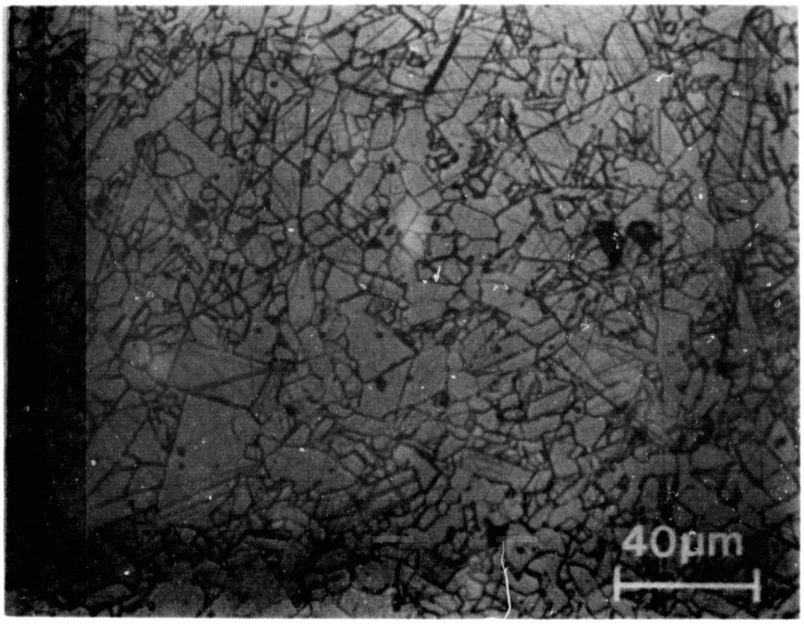

FIGURE 3: S. NO. 2-2-3. MICROSTRUCTURE OF ALPHA SILICON CARBIDE HOT PRESSED AT 2000°C

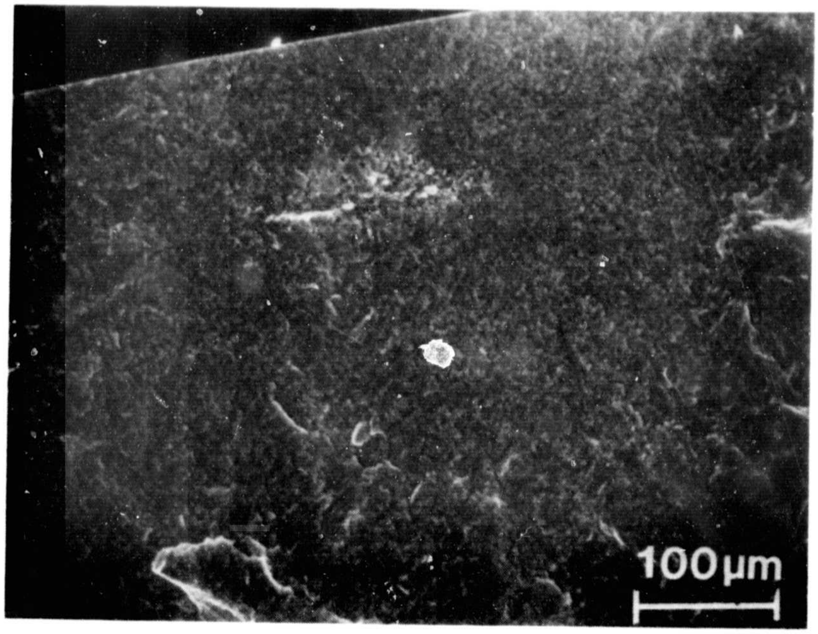

4(A)

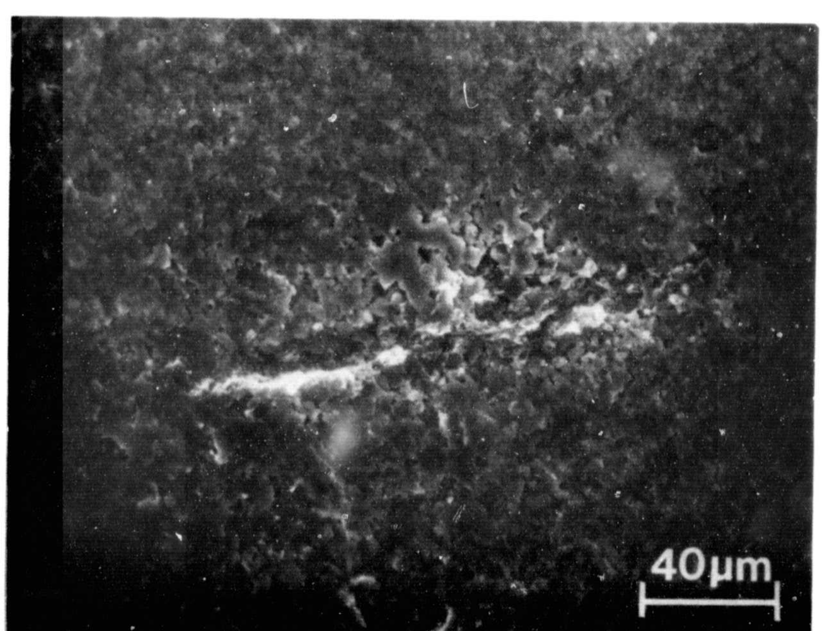

4(B)

FIGURE 4: FAILURE ORIGIN FOR A SPECIMEN HOT PRESSED AT 1800°C (σ_f = 82.91 KSI)

MP-74087

The reason why large size voids (125-250 µm) are not detected for 0.1-inch and 0.125-inch thick disks while medium size voids (50-125 µm) are detected cannot be explained. To the best of the knowledge of people who made these specimens, the specimen identification numbers are correct. We plan to do the following:

(a) Carefully section the medium size disks and examine the microstructure to measure the size of the detected voids; and

(b) Try lower voltage, better focus, and magnification to re-examine the disks with large voids.

The plates fabricated with medium and large size voids were also examined by microfocus x-ray. The plates were 0.25-inch thick. Whereas the large voids could be detected, the medium void disks were not detected. Test bars will be cut from these plates such that the voids are near the tensile surface when broken in a bend test.

Surface grinding and re-indentation are continuing for disk specimens which were returned from Sonoscan, Incorporated and Wayne State University after preliminary examination. These will be shipped to the above subcontractors next month.

3 - MECHANICAL PROPERTIES

3.1 - Stepped-Up Stress Rupture Tests

Failure analysis of the stepped-up stress rupture tested bars, reported in the April Monthly Report, is now available (See Table III). The specimens that broke after exposure to temperatures above 1300°C (namely, 4-11, 5-3, and 4-6) showed some fuzzy intergranular fracture region perhaps indicative of slow crack growth (via grain boundary sliding, for example) occurring at these temperatures (Figure 5). The nature of the failure origins for other specimens were not significantly different from those normally observed for alpha SiC broken at room temperature. In other words, no critical flaw modification occurs below the temperatures where

TABLE III

FAILURE ANALYSIS OF BARS TESTED BY STEPPED-UP RUPTURE TEST

S. No.	Fracture Stress, σ_f, 10^3 psi	Comments
2-1	55.0	Chamfer damage; failure occurred at 800°C after 0.8 h.
8-5	55.0	Surface-connected semi-elliptical void with surrounding porous region; a = 30 μm; c = 120 μm. Failure occurred at 800°C after 4.1 h.
5-7	55.0	Surface-connected semi-elliptical processing void; surrounding porous region. a = 26 μm; c = 120 μm. Failure occurred at 900°C after 7.35 h.
1-6	55.0	No obvious fracture origin. The specimen failed at 1100°C in 22.8 h.
4-11	50.0	Semi-elliptical surface void. a = 60 μm; c = 90 μm. Failed at 1300°C after 17.7 h.
5-3	50.0	Chamfer damage. Failed at 1300°C after 23.6 h.
4-6	40.0	Semi-circular poorly-bonded region. Failed at 1500°C after 2.1 h.

ORIGINAL PAGE
BLACK AND WHITE PHOTOGRAPH

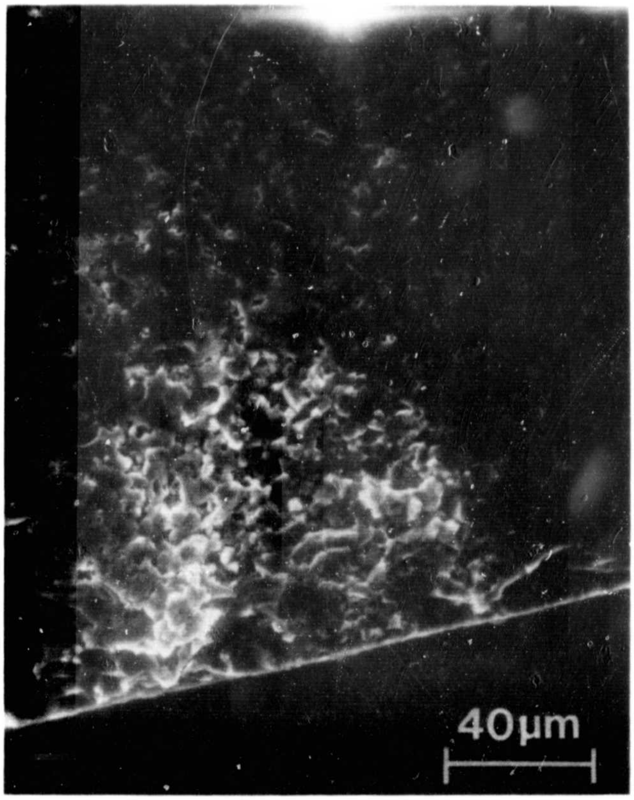

FIGURE 5: FAILURE ORIGIN FOR S. NO. 4-11. FAILED AT 1300°C AFTER 17.7 H. SURVIVED 24 HOURS SUCCESSIVELY AT 800°C THROUGH 1200°C AT 100°C INTERVALS.

slow crack growth becomes predominant. However, for conclusive evidence, many more specimens need to be tested.

3.2 - Baseline Properties Determination

3.2.1 - Injection Molded Alpha SiC

Failure analyses of specimens tested at room temperature (strength results reported in May Monthly Report) are now available.

The failure origins in the flexural specimens are identified whenever possible from the scanning electron micrographs of the fracture surfaces. The shape and size of the origin are defined by the major and minor axes ("2c" and "2a" respectively) of the encompassing elliptical or semi-elliptical area. The location of the flaw with respect to the specimen surface with the maximum applied tensile stress during bending is used to evaluate the stress at the fracture origin at failure. The flaws are categorized as follows:

Surface Flaws - Semi-elliptical flaw at the surface of the specimen, including breadthwise surfaces.

Subsurface Flaws - Elliptical flaw located just below the tensile surface (maximum depth arbitrarily set at 100 μm from the surface).

Internal Flaws - Elliptical flaw located at distances greater than 100 μm from the surface.

Corner Flaws - Fracture originating from the edges (may or may not be due to chamfering damage).

Whenever the flaw size determination is ambiguous, alternate measurements are also noted.

Tables IV and V give details of failure analysis including flaw size and location. Tables VI and VII give data on defect types and distributions in broken test bars. It is observed that surface and subsurface flaws govern the failure of injection molded alpha SiC for greater than 56 percent of test bars. Some examples of failure origins are shown in Figures 6 to 11. Figure 6 shows an internal flaw which is processing-related. This specimen had a flexural strength of 71,080 psi at surface, and 67,740 psi at flaw location. Figure 7 shows another processing-related flaw

TABLE IV

FAILURE ANALYSIS OF AS-RECEIVED INJECTION MOLDED ALPHA SIC BARS

SAMPLE: Injection Molded SASC, As-Furnaced

TEST TEMPERATURE: 25°C

Specimen No.	Fracture Stress, 10^3 psi		Description
	At Surface	At Flaw	
114	54.34	--	Fracture originating from chamfered edge.
120	48.39	48.39	Elliptical processing related, void connecting to surface; $a \approx 15$ µm, $c \approx 30$ µm.
124	63.27	63.27	A "delamination" crack 80 µm long, parallel to surface at 30 µm from the surface.
125	66.89	55.29	A large processing related void, 270 µm from the tensile surface; $a = 45$ µm, $c = 60$ µm.
126	48.25	48.25	Fracture originated from surface flaw 15 µm deep ("a") and 350 µm long ("2c").
127	37.73	37.73	A "delamination type" crack about 500 µm long running parallel to the surface at 40 µm from it.
128	55.70	55.70	A long "delamination" type crack (350 µm long) at 20 µm from the surface running parallel to it.
130	41.76	41.76	Originated at surface; no distinct failure originating flaw was found.

TABLE IV (Continued)

Specimen No.	Fracture Stress, 10^3 psi		Description
	At Surface	At Flaw	
131	52.75	45.97	Fracture originated near the chamfered edge in the lateral surface, 400 µm from the tensile surface.
132	52.80	52.80	A large semi-circular poorly bonded area at the surface, 200 µm in diameter.
133	52.79	52.79	Small elongated surface flaw, c = 40 µm, a = 10 µm.
176	37.26	37.26	Large surface flaw. c = 160 µm, a = 70 µm.
182	59.66	--	No apparent fracture origin found.
186	47.13	47.00	Large subsurface hole, tri-angular in shape; a = 35 µm, c = 75 µm.
187	48.77	48.77	Surface originated failure; No distinct fracture origin noticeable.
235	83.15	83.15	Small semi-elliptical surface flaw; a = 45 µm, c = 75 µm.
236	82.32	78.99	Small internal, circular void (processing related) near the chamfered surface; 40 µm in diameter, 125 µm from the tensile surface.
240	83.41	83.41	Surface originated failure; no distinct fracture origin is observed.

TABLE IV (Continued)

Specimen No.	Fracture Stress, 10^3 psi		Description
	At Surface	At Flaw	
241	69.09	69.09	Fracture originated from shallow surface irregularity, a = 25 µm, c = 90 µm.
242	60.09	60.09	Surface originated failure, no distinct origin can be observed.
243	73.16	73.16	Fracture originated from a shallow but long surface irregularity; a = 20 µm, c = 450 µm.
244	70.92	--	No apparent fracture origin found.
245	63.21	63.21	Large, deep subsurface void (processing related) close to the chamfered corner; a = 60 µm, c = 75 µm.
246	66.15	65.51	Spherical partially bonded agglomerate; 50 µm in diameter, 30 µm from the surface.
247	77.07	77.07	Small subsurface (surface-connected) flaw; a = 20 µm, c = 20 µm.
251	61.19	--	Surface originated failure; no distinct fracture origin found.
258	74.80	71.64	Internal, unbonded or partially bonded agglomerate; 50 µm in diameter, 130 µm from the tensile surface.

TABLE IV (Continued)

Specimen No.	Fracture Stress, 10^3 psi		Description
	At Surface	At Flaw	
266	54.42	50.02	Internal processing related void, a = 45 μm, c = 50 μm, 250 μm from the surface.
273	50.23	--	Surface originated failure; no distinct fracture origin can be observed.
277	47.92	40.92	Processing void, 450 μm from the tensile surface, a = 20 μm, c = 20 μm.

TABLE V

FAILURE ANALYSIS OF ANNEALED INJECTION MOLDED ALPHA SIC BARS

SAMPLE: IM SASC - Annealed

TEST TEMPERATURE: 25°C

Specimen No.	Fracture Stress, 10^3 psi		Description
	At Surface	At Flaw	
42	57.74	53.74	Internal processing void, 215 µm from the tensile surface; a = 30 µm, c = 40 µm.
43	44.24	41.54	Large internal void with sharp corners, 190 µm from tensile surface; a = 35 µm, c = 65 µm.
44	47.64	47.18	Small circular subsurface void (diameter = 30 µm), 30 µm from surface.
45	45.33	45.33	Cluster of two voids and unbonded area adjacent to them; forming a semi-elliptical surface flaw; a = 45 µm, c = 48 µm.
51	40.56	40.56	Unbonded area in the corner near the chamfered edge.
53	66.34	66.34	Very small surface flaw, a = 10 µm, c = 35 µm.
54	74.05	71.16	Internal void oriented at an angle to fracture surface; 120 µm from the tensile surface; a = 25 µm, c = 35 µm.
55	73.29	67.83	Large porous area at 230 µm from tensile surface; approximately 150 µm in diameter.

TABLE V (Continued)

Specimen No.	Fracture Stress, 10^3 psi		Description
	At Surface	At Flaw	
93	55.69	55.69	Processing void very close to surface at one end; a = 25 µm, c = 40 µm.
94	46.30	--	Corner originated failure; no specific origin found.
98	53.67	53.67	Large semi-elliptical surface flaw; a = 50 µm, c = 150 µm.
99	48.93	48.63	Failure originated at surface but no specific origin can be found.
103	56.58	56.58	Failure originated at chamfered edge; no flaw origin found.
110	58.47	53.32	Large unbonded agglomerate; 275 um from the surface; a = 40 µm, c = 50 µm.
111	62.55	61.55	Unbonded agglomerate at 50 µm from the surface (subsurface flaw); a = 10 µm, c = 40 µm.
191	55.09	55.09	Failure initiated at corner; due to chamfer damage.
192	70.71	69.56	Large subsurface void, 50 µm from tensile surface; a = 25 µm, c = 50 µm.
193	73.52	73.52	Semi-elliptical surface flaw; a = 40 µm, c = 200 µm.
194	69.69	--	No apparent failure origin found.

TABLE V (Continued)

Specimen No.	Fracture Stress, 10^3 psi		Description
	At Surface	At Flaw	
195	57.30	56.74	Subsurface void, 30 µm from tensile surface; triangular in shape; approximate 50 µm each side.
197	62.38	62.38	Surface originated failure but no specific fracture origin found.
198	71.45	71.45	Large semi-circular surface flaw; diameter 40 µm.
199	77.27	77.27	Failure originated at surface near chamfered edge, but no specific flaw can be located.
201	77.78	77.78	Failure originated at surface but no specific flaw found.
206	61.99	61.29	Circular subsurface flaw, 35 µm from surface, 60 µm in diameter.
209	53.02	45.33	A large unbonded region located at about 450 µm from the tensile surface; a = 110 µm, c = 175 µm.
215	63.24	--	No apparent fracture origin found.
219	68.99	66.99	Small "circular" unbonded agglomerate, 40 µm in diameter, 90 µm from the tensile surface.
225	71.08	67.74	Internal flaw at 140-150 µm from the tensile surface; a = 35 µm, c = 40 µm.
234	78.62	--	Small semi-elliptical flaw in the chamfered corner.

TABLE VI

DEFECT TYPES AND DISTRIBUTIONS IN FLEXURAL STRENGTH SPECIMENS

INJECTION MOLDED SASC - AS RECEIVED
TESTED AT 25°C

TYPE	NUMBER	PERCENT
Surface Flaws*	22	73
Internal Flaws	5	17
Corner Flaws**	1	3
Others†	2	7
TOTAL	30	100

TABLE VII

DEFECT TYPES AND DISTRIBUTIONS IN FLEXURAL STRENGTH SPECIMENS

INJECTION MOLDED SASC - ANNEALED
TESTED AT 25°C

TYPE	NUMBER	PERCENT
Surface Flaws*	17	57
Internal Flaws	7	23
Corner Flaws**	4	13
Others†	2	7
TOTAL	30	100

* Includes subsurface origins (located within 100 um from the tensile surface) and surface originated failure without any specific origin.

** Includes chamfer damage.

† No apparent fracture origin found.

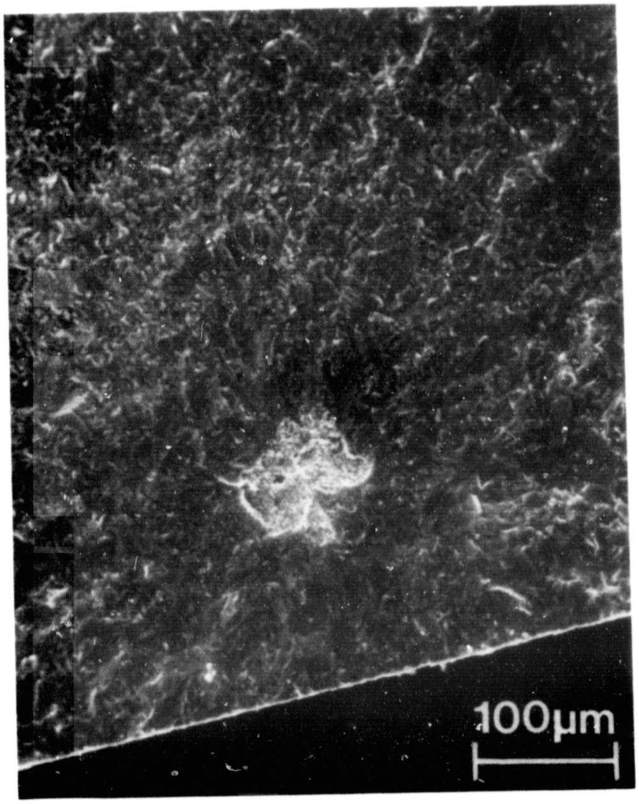

FIGURE 6: INTERNAL DEFECT AS FAILURE ORIGIN FOR SPECIMEN NO. 225, σ_f = 71.1 KSI.

ORIGINAL PAGE
BLACK AND WHITE PHOTOGRAPH

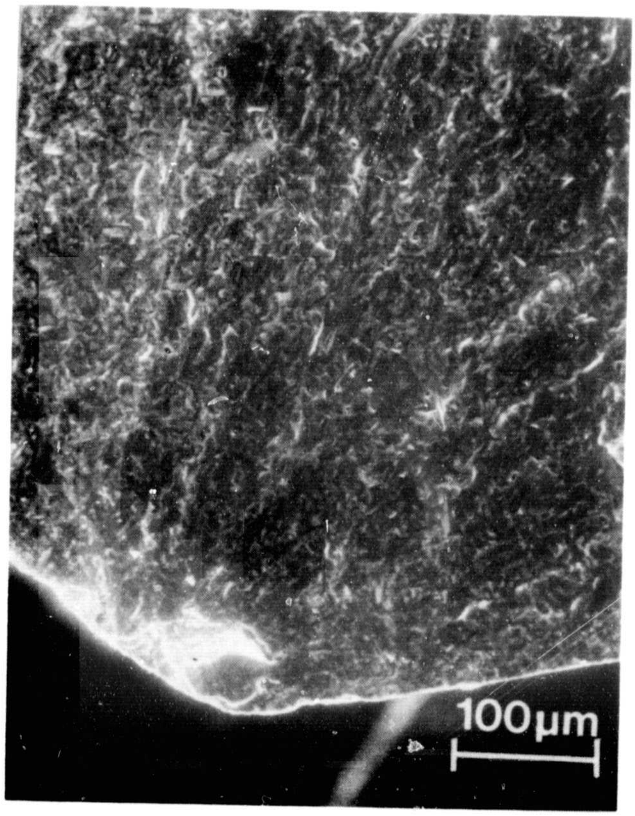

FIGURE 7: PROCESSING FLAW AT CHAMFER EDGE FOR S. NO. 51, σ_f = 40.6 KSI.

ORIGINAL PAGE
BLACK AND WHITE PHOTOGRAPH

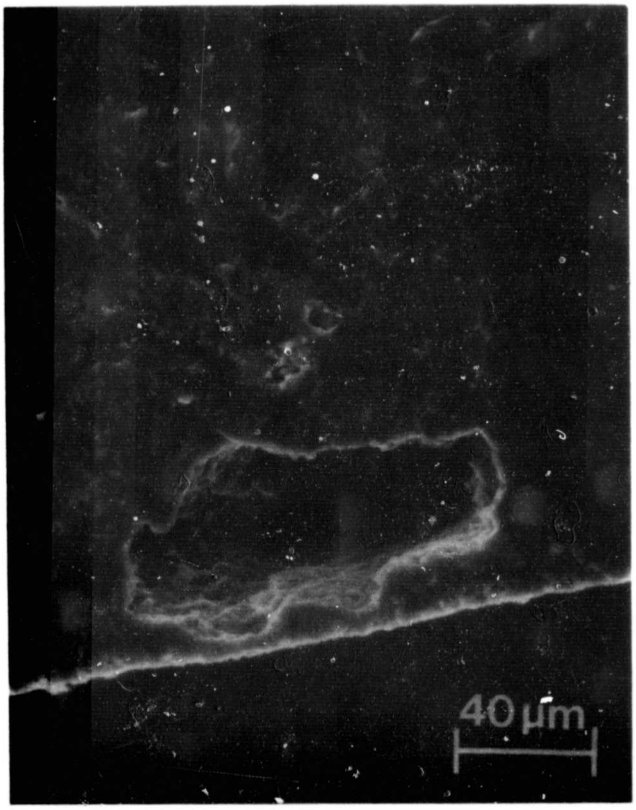

FIGURE 8: VOID AT THE SURFACE OF S. NO. 192. σ_f = 70,710 PSI. THE SPECIMEN WAS ANNEALED PRIOR TO ROOM TEMPERATURE TEST.

ORIGINAL PAGE
BLACK AND WHITE PHOTOGRAPH

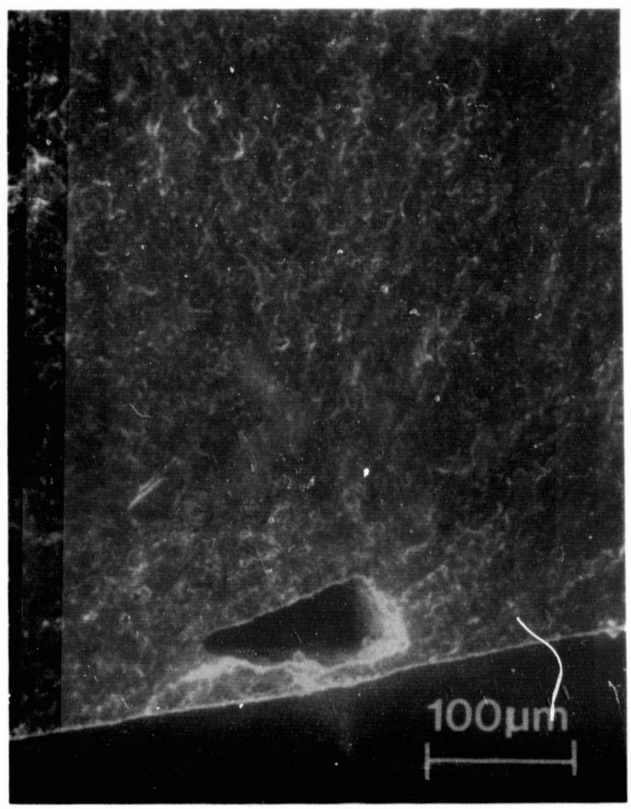

FIGURE 9: PROCESSING FLAW CLOSE TO TENSILE SURFACE OF S. NO. 186. σ_f = 47,130 PSI

MP-74085

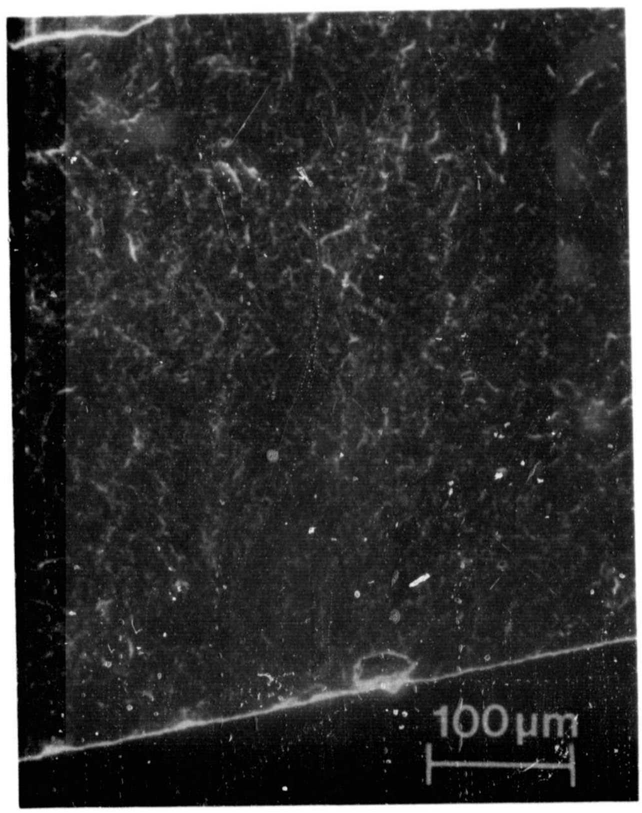

FIGURE 10: FAILURE ORIGIN FOR S. NO. 247.
σ_f = 77.1 KSI.

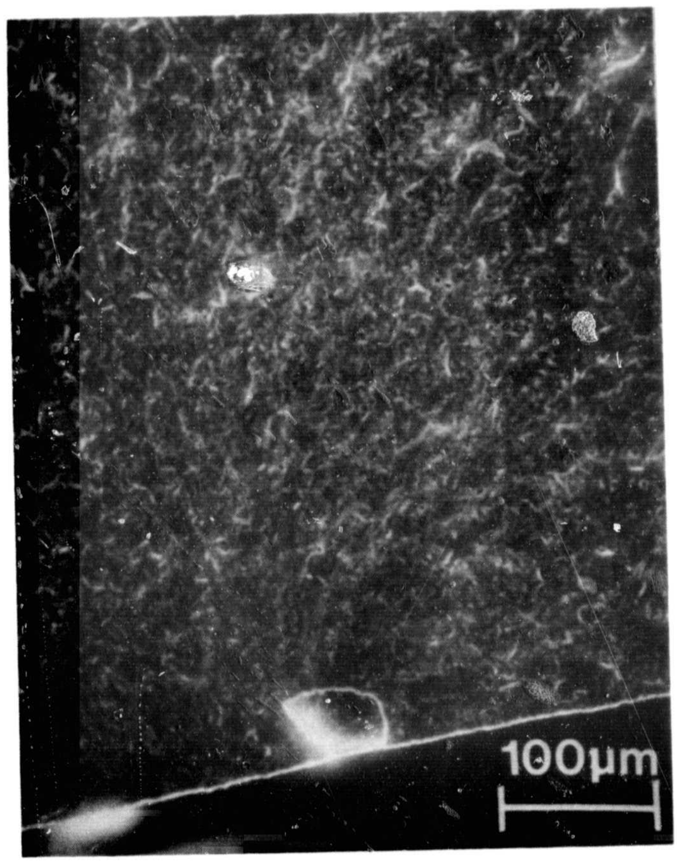

FIGURE 11: PROCESSING-RELATED SURFACE VOID AS FRACTURE ORIGIN FOR S. NO. 120. σ_f = 48.4 KSI

located at chamfer edge. This specimen had a flexural strength of 40,560 psi. Figure 8 shows a large surface flaw controlling the strength of a specimen. Even though this is a large flaw, the specimen strength was 70,710 psi. However, yet another specimen had a strength of 47,130 psi for a similar flaw size (Figure 9). However, S. No. 192 was annealed before testing whereas S. No. 186 was tested in the as-received condition. This observation might suggest the beneficial effect of annealing. But no conclusive evidence is available. For example, S. No. 247, whose failure origin is shown in Figure 10, had a strength of 77,070 psi. S. No. 120, whose failure causing flaw size is similar (Figure 11) exhibited a strength of only 48,390 psi. Both specimens were tested in the as-received condition. An etched microstructure of injection molded alpha SiC (S. No. 176, σ_f = 37.26 ksi) is shown in Figure 12.

In summary, the majority of failure-causing flaws are processing-related. Although the fracture mechanics concept of increased material strength with decreasing flaw size was generally observed, occassional exceptions were also seen. Failure analysis also fails to provide reasons for the beneficial effects on strength observed on annealed specimens.

3.3 - Strength Tests

Both slip cast alpha SiC (standard fine grained mix) and cold pressed alpha SiC were tested for strength at 1200°C (2192°F). The bars had average cross section of 0.125" x 0.25" and were tested in 4-point bend by using 0.75" inner span and 1.5" outer span.

The slip cast alpha SiC results are shown in Table VIII and in the form of a Weibull plot in Figure 13. The average strength was 61.15 $\pm$ 9.71 ksi. Lowest strength was 38,060 while a high strength of 79,800 was also seen.

The cold pressed alpha SiC results are shown in Table IX and in the form of a Weibull plot in Figure 14. The average strength was 51.21 $\pm$ 7.09 ksi. The lowest strength was 37,350 psi and the highest strength was 66,820 psi.

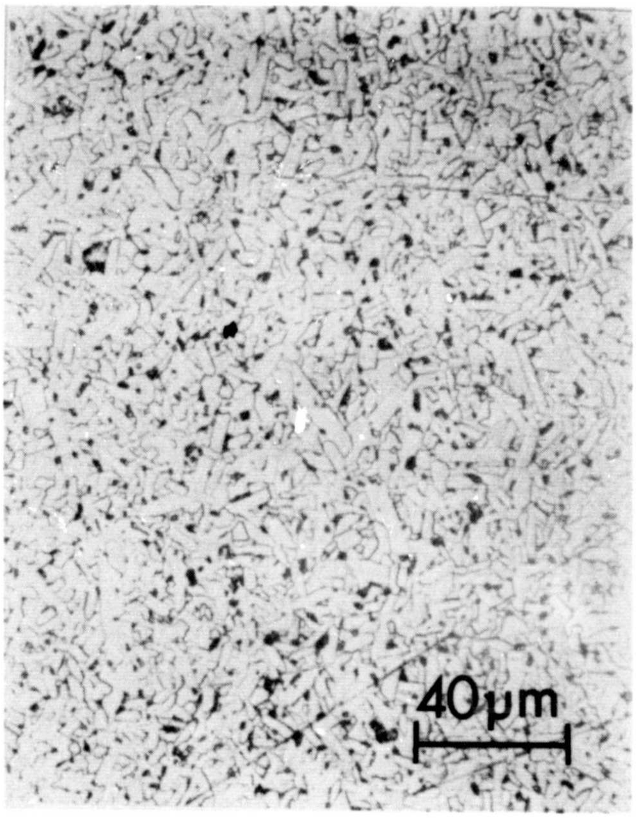

FIGURE 12: ETCHED MICROSTRUCTURE OF INJECTION MOLDED SINTERED ALPHA SiC

C-2

MP-74090

TABLE VIII

FLEXURAL STRENGTH OF SLIP CAST ALPHA SIC 1200°C

Sample	σ_f ksi
36-1-1	38.06
36-1-3	55.03
36-7-3	74.02
36-13-1	63.57
36-14-3	74.86
37-1-1	67.49
37-1-3	64.81
37-1-4	70.15
37-1-6	69.87
37-3-1	59.48
37-3-2	62.50
37-3-3	68.50
37-3-4	61.29
37-3-5	73.64
37-4-1	79.80
37-4-2	66.11
37-5-5	64.31
37-6-2	61.44
37-6-3	58.45
37-11-2	55.26
37-12-1	43.84
37-13-6	51.60
37-13-7	49.42
37-13-10	60.63
37-14-1	61.13
37-14-2	46.23
37-14-3	56.10
37-14-4	52.73
37-14-6	69.37
37-14-8	54.71

Average Strength = 61.15 ksi
Standard Deviation = 9.71 ksi
Charac. Strength = 65.38 ksi
(k=1, for specimen volume)
Weibull Modulus = 6.70

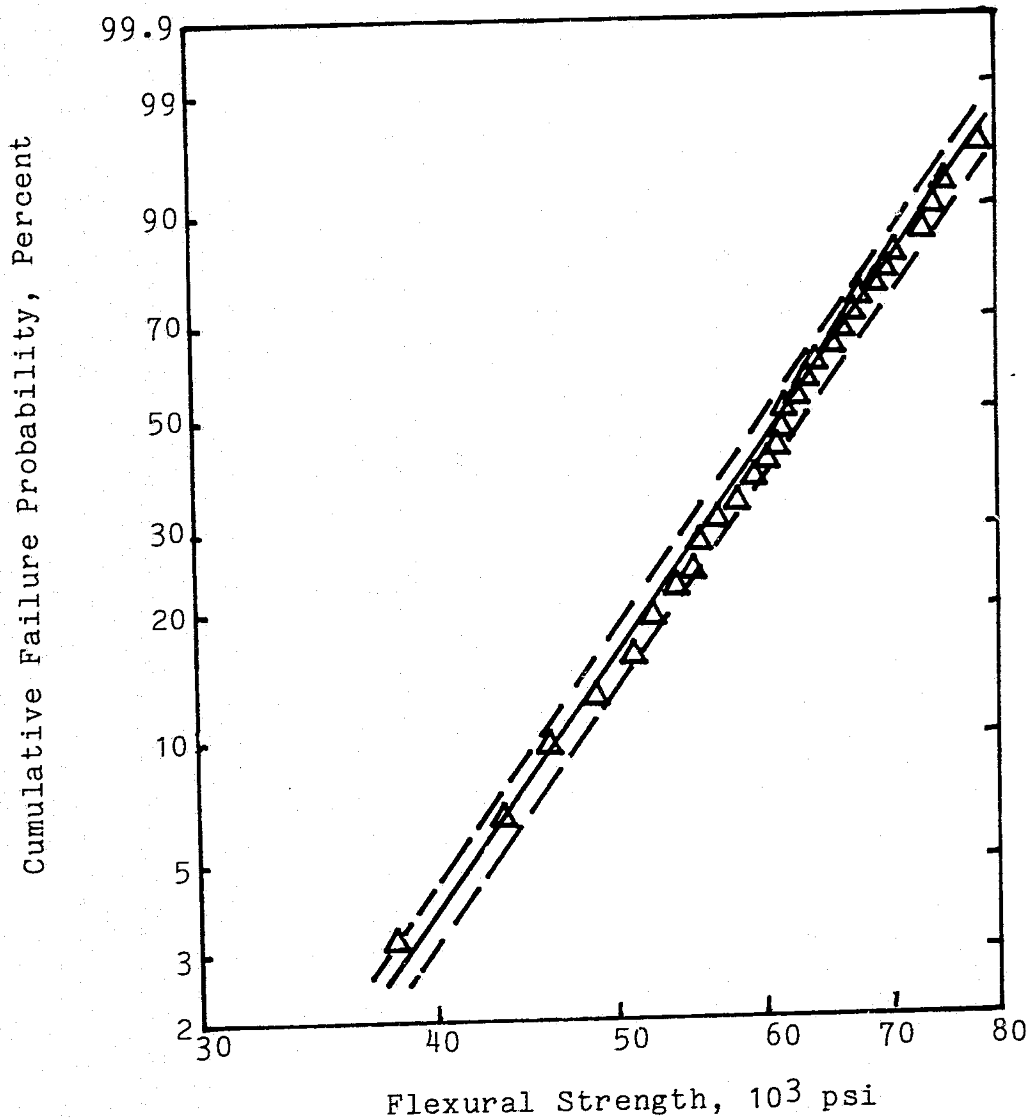

FIGURE 13: WEIBULL DISTRIBUTION OF STRENGTH DATA FOR SLIP CAST ALPHA SIC AT 1200°C (2192°F)

TABLE VII

FLEXURAL STRENGTH OF DRY PRESSED SASC AT 1200°C

Sample	σ_f ksi
D454-51-23-9	38.81
23-10	38.55
21-8	44.34
10-9	48.07
10-10	50.86
12-3	53.61
12-6	63.88
12-8	43.12
12-9	37.30
12-12	46.16
1-1	51.58
1-2	55.48
1-5	49.07
1-6	51.36
1-7	50.63
1-8	53.47
1-9	60.07
4-9	47.87
11-1	51.47
11-2	58.28
11-5	61.66
11-9	46.69
14-1	51.66
14-5	45.37
14-7	50.61
14-9	58.97
15-5	55.63
15-7	51.82
15-8	50.16
15-9	66.82
15-10	53.47

Average Strength = 51.21 ksi
Standard Deviation = 7.09 ksi
Charac. Strength = 54.30 ksi
(k=1, for specimen volume)
Weibull Modulus = 7.89

ORIGINAL PAGE IS
OF POOR QUALITY

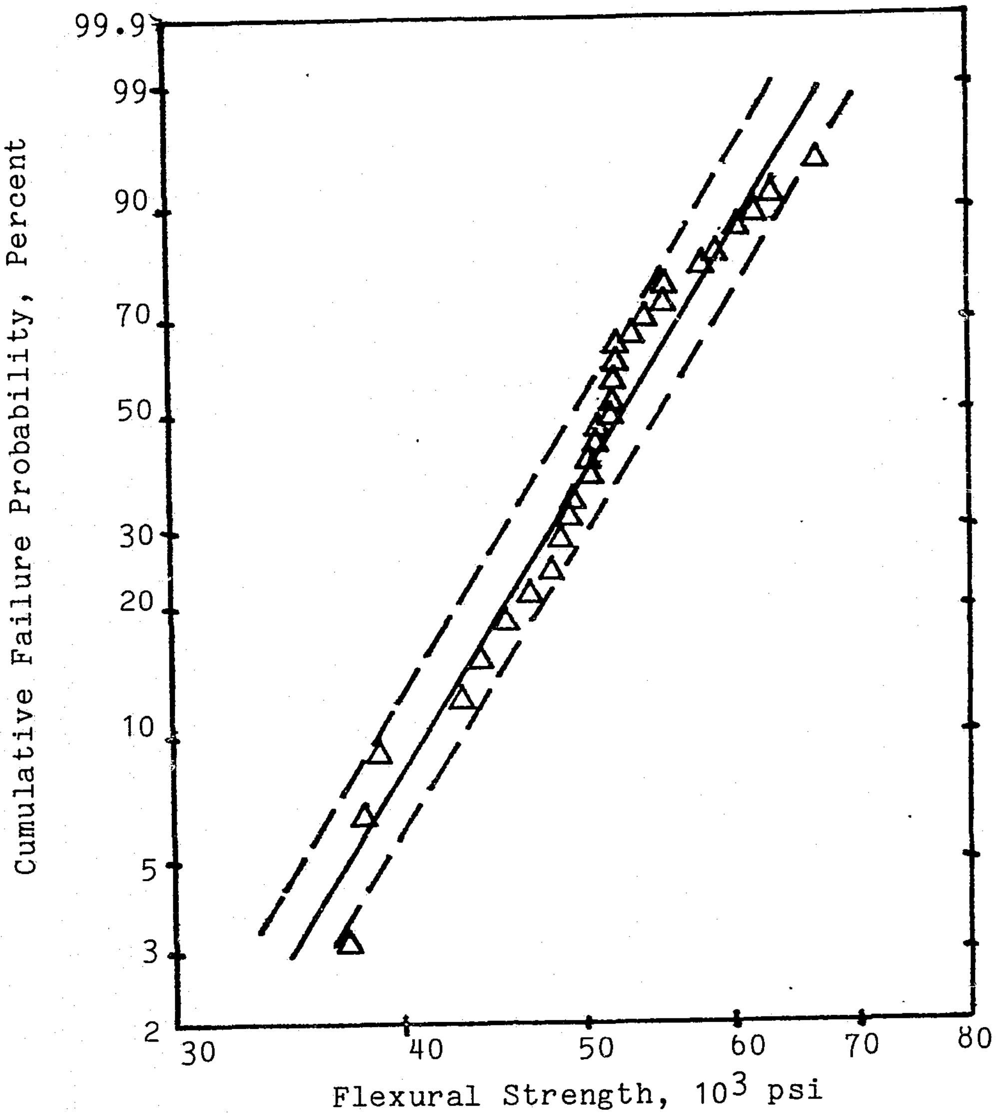

FIGURE 14: WEIBULL DISTRIBUTION OF STRENGTH DATA FOR COLD PRESSED ALPHA SIC AT 1200°C (2192°F)

APPENDIX IV

CARBORUNDUM UNIQUE DEVELOPMENT WORK

AIRESEARCH MANUFACTURING COMPANY OF ARIZONA

ADVANCED GAS TURBINE (AGT) PROGRAM

CARBORUNDUM UNIQUE WORK

SUMMARY REPORT NO. 9

TO AUGUST 31, 1980

SEPTEMBER 9, 1980

JOHN CHEW
SENIOR PROJECT MANAGER

THE CARBORUNDUM COMPANY
ALPHA SILICON CARBIDE DIVISION
P.O. BOX 832
NIAGARA FALLS, NEW YORK 14302

1 - CERAMIC TURBINE ROTOR (BCC)

Progress towards the fabrication of a solid simulated rotor using bonding techiques continued during this period. Presintered SiC shells were joined to presintered SiC cores using a sinterable SiC compound at the interface. The application of heat and pressure to the assembly resulted in the development of a good dense bond between the components.

To date, a total of 13 hot pressing attempts resulting in 11 simulated rotors were prepared using this technique. Seven of these were described in previous reports. The balance, identified by notebook number, are described here.

D655-32 identifies the first attempt during this period. The procedure used a vacuum de-airing step prior to isopressing the segments with the sinterable SiC at the interface. During the subsequent hot pressing operation, the mold ruptured before achieving maximum temperature and pressure. The mold had been used in several pressing attempts and failure is attributed to fatigue.

D655-33 used the assembly prepared for the previous run. A prior attempt at repressing had been unsuccessful; but in this case, a good bond was produced. A view of the cross-section is shown in Figure 1.

D655-34 was the first simulated rotor consisting of the thin wall shell configuration and the corresponding core shape. The core insert, in this case, was machined to provide the spherical contour at the hub base. The component assembly scheme is shown in Figure 2. The hot pressing technique was the same as that used for the previous rotor D655-33. This rotor, however, when sectioned revealed porosity in the same regions of the assembly where it was seen in some of the earlier rotors. It was concluded that insufficient sinterable SiC was available for compaction during the isopressing step.

D655-35 also used the thin wall shell with the new core shape. In order to overcome the porosity problem previously encountered, a large excess of sinterable mix was applied to the shell prior to insertion of the core. The excess mix was used to ensure the removal of entrapped air. The assembly was hot pressed at the same temperature and pressure used in the prior run. Except for surface imperfections at the exterior bond interface, the part looked good. The whole bonded rotor assembly is shown in Figure 3. No internal porosity was detected from the x-ray analysis. It should be mentioned that the core material used for this sample rotor was not optimized with respect to strength but was used to demonstrate fabricability. Nevertheless, discussions by Airesearch and Carborundum personnel resulted in a decision to spin the part to failure. From this test and the subsequent fracture analysis, it is hoped to learn whether the bond or the core material is the limiting factor at this point in the rotor development program. Microstructures and characteristic strengths for the core material are being determined at the present time.

D655-36 is a repeat of D655-35. The hot pressed assembly is currently undergoing NDE.

D655-37 used a core consisting of 3 separate segments. The same bonding procedure was used to join the components. The hot pressed rotor assembly is shown in Figure 4. NDE is being carried out for this part. There didn't appear to be any significant fabrication advantages using this approach, therefore, it will not be pursued further.

The feasibility of producing the simulated rotor using RBSiC via the thixotropic casting method has been demonstrated. A fully cured, crack-free rotor has been made and siliconized. Minor voids were visible at the large end but no other flaws were apparent. Another rotor was cast over-length and faced off to remove surface voids. Siliconizing is scheduled for mid-September.

A new rubber mold with increased overall length was fabricated. The cast part will then be long enough to allow machining of the spherical radius at the base of the rotor. Casting development in this new mold is in progress.

2 - CERAMIC STRUCTURES

2.1 - Stator Segment L3846162

Delivery of the injection molding tool is expected in mid-September.

2.2 - Shroud, Turbine L3846151

Delivery of injection molding tool expected end of September.

2.3 - Combustor Baffle L3846149

Model has been received and is shown in Figure 5.

2.4 - Diffuser Inner, L3846156

Model has been received and is shown in Figure 6.

2.5 - Transition Duct L3846159

Model has been ordered.

2.6 - Diffuser, Outer L3846161

Model has been ordered.

2.7 - Spacer, Duct L3846150

First articles have been shipped to grinding vendor for final machining.

2.8 - Shield, Regenerator L3846154

Green machining complete. First articles have been sintered and are being inspected prior to final grinding.

2.9 - Backshroud, Turbine L3846148

Billets have been isopressed. A breakdown in the mimic apparatus in green machining has prevented completion as originally scheduled. A new schedule will be developed when repairs are made.

FIGURE 1: CROSS SECTION OF SIMULATED ROTOR D655-33

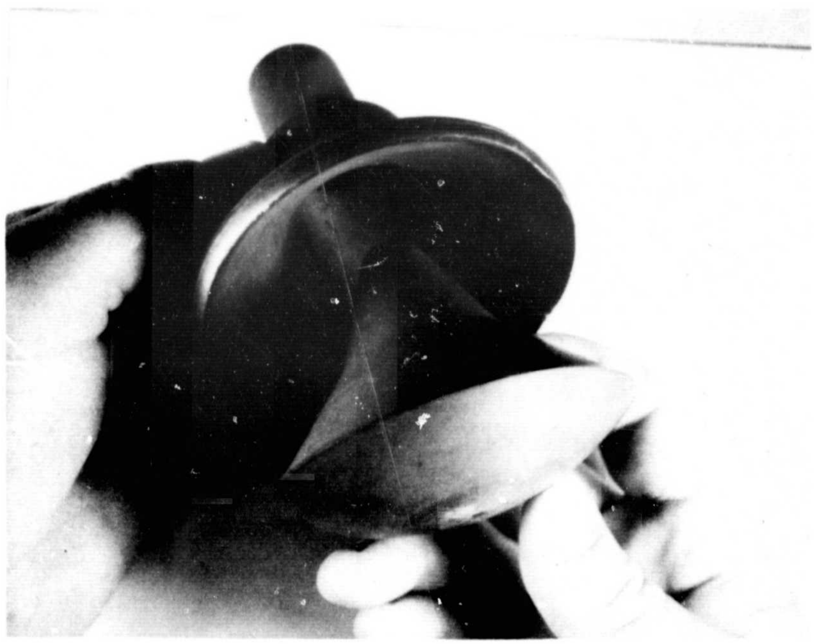

FIGURE 2: COMPONENT ASSEMBLY SCHEME FOR SIMULATED ROTOR

FIGURE 3: HOT PRESSED ROTOR ASSEMBLY D655-35

ORIGINAL PAGE
BLACK AND WHITE PHOTOGRAPH

FIGURE 4: HOT PRESSED SIMULATED ROTOR WITH 3 SEGMENT CORE

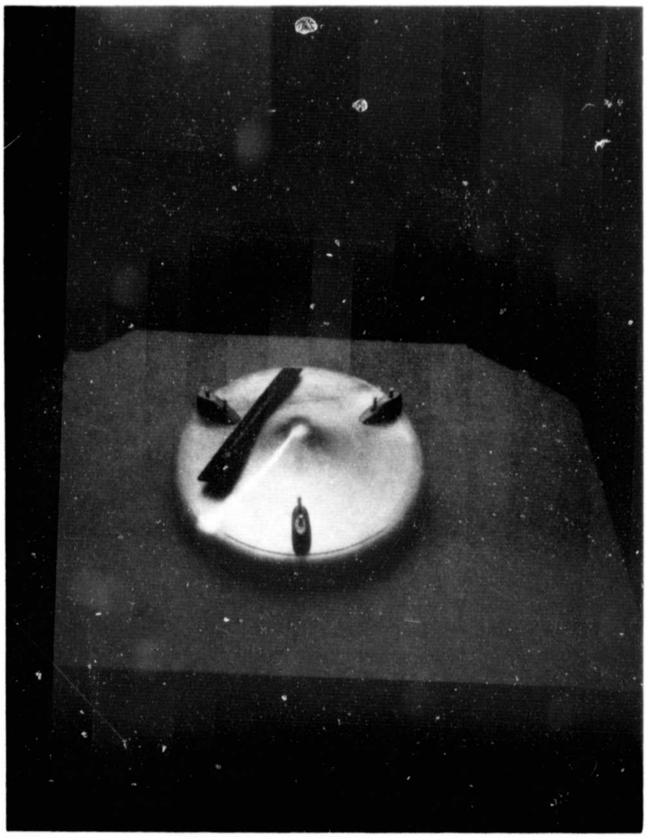

FIGURE 5: COMBUSTOR BAFFLE MODEL

AIRESEARCH MANUFACTURING COMPANY OF ARIZONA
A DIVISION OF THE GARRETT CORPORATION
PHOENIX, ARIZONA

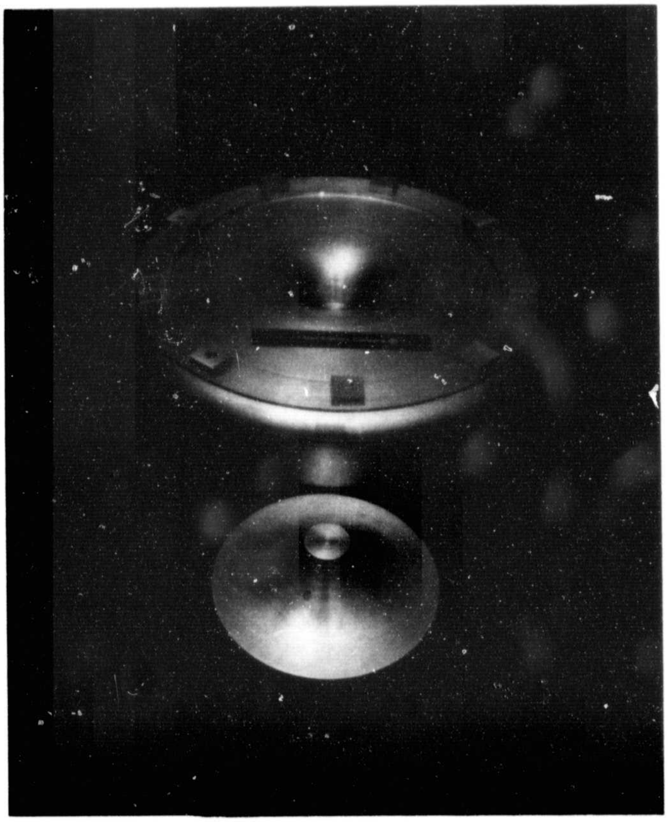

FIGURE 6: MODEL FOR INNER DIFFUSER

DEVELOPMENT SCHEDULE

SLIPCAST STRUCTURES

		MODEL QUOTES	MODEL ORDER	MODEL RECEIVED	MOLD FABRICATION	CASTING	MOLD REWORK	CASTING	DRYING	FIRING FIXTURES	FIRING	INSPECTION	MACHINING	INSPECTION	SHIP	COMMENTS
COMBUSTOR, BAFFLE	Est.	5-30	6-15	8-20	8-30	9-8	9-15	9-22 11-30	9-30 12-15	9-30 12-30	10-15 1-15	10-15 1-30	1-15 2-30	1-30 3-15	2-15 3-30	
L3846149	Act.	6-5	7-15	8-20												
DIFFUSER, INNER	Est.	6-15	6-30	8-20	8-30	9-15	9-22	9-30 12-1	10-6 12-15	10-6 12-15	10-15 1-30	10-15 1-30	1-15 2-28	1-30 3-15	2-15 3-30	
L3846156	Act.	6-20	7-14	8-20												
TRANSITION DUCT	Est.	5-30	6-15	7-30	8-15	8-22	8-30	9-5 11-15	9-15 12-1	9-15 12-1	9-30 12-30	9-30 1-15	12-30 2-15	1-15 3-1	1-30 3-15	Model Late
L3846159	Act.	6-5	6-27			8-22										
DIFFUSER, OUTER	Est.	5-30	6-15	7-30	8-15	8-22	8-30	9-5 11-15	9-15 12-1	9-15 12-15	9-30 12-30	9-30 1-15	12-30 2-15	1-15 3-1	1-30 3-15	Model Late
L3846161	Act.	6-5	6-27													

NOTE: WHERE TWO DATES ARE SHOWN, THE FIRST INDICATES COMPLETION OF FIRST ARTICLES, THE SECOND INDICATES COMPLETION OF FINAL ARTICLES.

ORIGINAL PAGE IS
OF POOR QUALITY

DEVELOPMENT SCHEDULE

MACHINED STRUCTURES

		ISOPRESS BILLETS	GREEN MACHINE	SINTER	INSPECTION	GRINDING	FINAL INSPECTION	SHIP	COMMENTS
SPACER DUCT L3846150	Est.	6-18	7-21	7-28	8-6	8-22	8-27	9-2	
	Act.	6/19	7-28	8-15	9-5				
SHIELD REGENERATOR L3846154	Est.	7-21	8-6	8-15	8-21	9-5	9-11	9-12	
	Act.	7-28	8-20						
BACKSHROUD, TURBINE L3846148	Est.	7-11	7-23	7-31	8-6	9-19	9-24	9-30	Revised schedule - tooling
	Act.	8-15							

NOTE: WHERE TWO DATES ARE SHOWN, THE FIRST INDICATES COMPLETION OF FIRST ARTICLES, THE SECOND INDICATES COMPLETION OF FINAL ARTICLES.

DEVELOPMENT SCHEDULE

INJECTION MOLDED STRUCTURES

		TOOL QUOTES	TOOL ORDER	TOOL RECEIVED	TOOL CHECK	REWORK	RECHECK	MOLDING	BAKING	SINTERING	NDE	GRINDING	NDE	SHIP	COMMENTS
STATOR SEGMENT	Est.	6-2	6-9	9-22	9-29	10-13	10-20	10-27 11-24	11-10 12-15	11-17 12-31	11-24 1-15	12-29 2-2	1-15 2-16	1-30 3-2	No Changes
L3846162	Act.	6-9	6-13												No Changes
SHROUD TURBINE	Est.	6-2	6-9	10-27	11-3	11-17	11-24	12-1 12-22	12-22 1-12	1-16 2-2	1-23 2-16	2-20 3-16	2-27 3-30	3-6 4-6	No Changes
L3846151	Act.	6-16	6-25												No Changes

NOTE: WHERE TWO DATES ARE SHOWN, THE FIRST INDICATES COMPLETION OF FIRST ARTICLES, THE SECOND INDICATES COMPLETION OF FINAL ARTICLES.

ORIGINAL PAGE IS OF POOR QUALITY

ORIGINAL PAGE IS
OF POOR QUALITY

FEASIBILITY/DEVELOPMENT SCHEDULE

SIMULATED ROTOR

		MOLDING	BAKING	SINTERING	TOOL ORDER	TOOL RECEIVED	INSERT MANUFACTURE	NDE ON SEGMENTS	HOT PRESSING	NDE FINAL	SHIP	COMMENTS
SOLID ROTOR	Est.	9-10	10-10 11-10	10-17 11-17	N/A	N/A	N/A	N/A	N/A	11-21 12-15	11-28 12-19	Injection Molding Tool to be Modified
	Act.											
ROTOR WITH DENSE SIC INSERTS	Est.	6-23	5-8 7-28	5-16 8-4	5-30 6-17	6-9 7-8	5-23 7-21	7-21 7-24	7-31 9-30	9-30 10-30	10-2 11-4	New Molds Required Due to Low Density Graphite Stock
	Act.		5-8	5-16	5-30	7-9	5-23	7-24 --	8-14 --	8-21 --	8-25 --	
ROTOR WITH SINTERABLE POWDER INSERT	Est.		5-8	5-16	5-30	7-9	7-21	N/A	8-8	8-30	9-1	Isopressing Bags Wore Out, Ordered New Bags
	Act.		5-8	5-16	5-30	7-9			8-8 --			
ROTOR WITH REACTION BONDED SIC INSERT	Est.		5-8	5-16	5-30	7-9	7-21	N/A	8-15	9-15	9-19	Isopressing Bags Wore Out, Ordered New Bags
	Act.		5-8	5-16	5-30		7-21 --					

8-15

NOTE: WHERE TWO DATES ARE SHOWN, THE FIRST INDICATES COMPLETION OF FIRST ARTICLES, THE SECOND INDICATES COMPLETION OF FINAL ARTICLES.